

Reward Distance Comparisons Under Transition Sparsity

Anonymous authors

Paper under double-blind review

Abstract

Reward comparisons are vital for evaluating differences in agent behaviors induced by a set of reward functions. Most conventional techniques employ optimized policies to derive these behaviors; however, learning these policies can be computationally expensive and susceptible to safety concerns. Direct reward comparison techniques obviate policy learning but suffer from transition sparsity, where only a small subset of transitions are sampled due to data collection challenges and feasibility constraints. Existing state-of-the-art direct reward comparison methods are ill-suited for these sparse conditions since they require high transition coverage, where the majority of transitions from a given coverage distribution are sampled. When this requirement is not satisfied, a distribution mismatch between sampled and expected transitions can occur, introducing significant errors. This paper introduces the Sparsity Agnostic Reward Distance (SARD) pseudometric, designed to eliminate the need for high transition coverage by accommodating diverse sample distributions, likely common under transition sparsity. We provide theoretical justifications for SARD’s robustness and conduct empirical studies to demonstrate its practical efficacy across various domains, namely Gridworld, Bouncing Balls, Drone Combat, and StarCraft 2.

1 Introduction

In sequential decision problems, reward functions often serve as the most “succinct, robust, and transferable” representations of a task (Ng & Russell, 2000), encapsulating agent goals, social norms, and intelligence (Silver et al., 2021; Zahavy et al., 2021; Singh et al., 2009). For problems where a reward function is specified and the goal is to find an optimal policy that maximizes cumulative rewards, Reinforcement Learning (RL) is predominantly employed (Sutton & Barto, 2018). Conversely, when a reward function is complex or difficult to specify, and past expert demonstrations (or policies) are available, the reward function can be learned via Inverse Reinforcement Learning (IRL) (Ng & Russell, 2000).

In both RL and IRL contexts, reward functions govern agent decision-making, and reward comparisons can help assess the similarity of these functions in terms of the behaviors that they induce. These comparisons could be useful for: (1) *Evaluating Agent Behaviors* – By comparing how different reward functions align or differ through specified similarity measures, agent rewards can be grouped (clustering) or categorized (classification), to reason and interpret the agents’ behaviors. This can be useful in IRL domains, where there is need to extract meaning from intrinsic rewards computed to represent agent preferences and motivations (Ng & Russell, 2000). For instance, in sport domains such as hockey, reward comparisons could be useful in inferring player rankings and their decision-making strategies (Luo et al., 2020). (2) *Initial Reward Screening* – In RL domains, direct reward comparisons (without computing policies) could serve as a preliminary step to quickly identify rewards that will achieve a spectrum of desired behaviors before actual training. This could be beneficial in scenarios where multiple possible reward configurations exist, but some might be more efficient. For example, it might be important to distinguish rewards that support defensive versus offensive strategies in military scenarios (Van Evera, 1998), or competitive versus cooperative behaviors in team settings (Santos & Nyanhongo, 2019). (3) *Addressing Reward Sparsity*¹ – Reward comparisons could also tackle issues such as reward sparsity, by identifying more informative, and easier-to-learn reward functions, that might be similar in terms of optimal policies but more desirable than sparse reward functions.

¹Transition sparsity arises when a minority of transitions are sampled. This is different from the concept of reward sparsity, which occurs when rewards are infrequent or sparse, making RL tasks difficult.

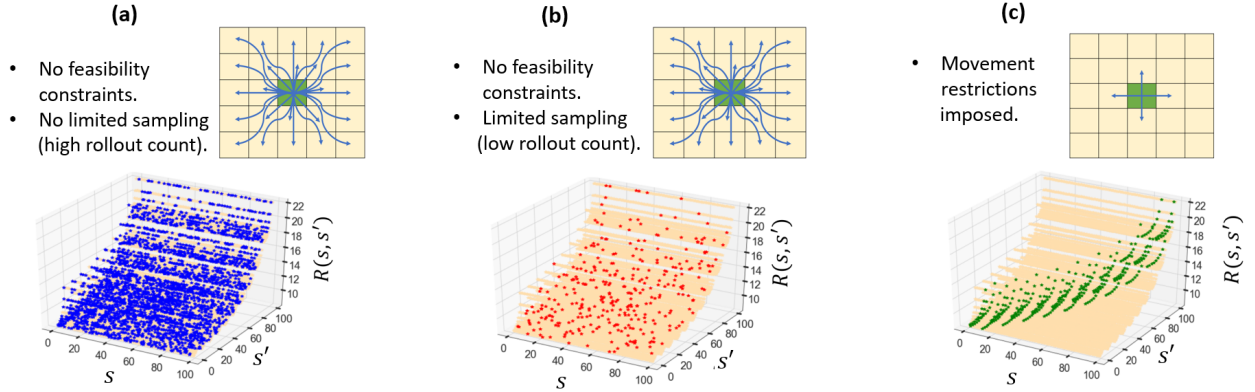


Figure 1: (Transition Sparsity in a 10×10 Gridworld Domain) In this illustration, each transition starts from a starting state s and ends in a destination state s' . For clarity in visualization, we consider action-independent rewards such that actions can be omitted, $R(s, s')$. In (a), high transition coverage results from a high rollout count (number of policy rollouts) in the absence of feasibility constraints, leading to the majority of transitions being sampled (blue points). In (b), low coverage results from a low rollout count in the absence of feasibility constraints, leading to fewer sampled transitions (red points). In (c), low coverage results from feasibility constraints, such as movement restrictions that only allow actions to adjacent cells; which can significantly reduce the space of sampled transitions (green points) irrespective of rollout count.

The task of reward comparisons aims to identify the similarity among a collection of reward functions. This can be done through pairwise comparisons where the similarity distance $D(R_A, R_B)$ between two reward functions, R_A and R_B (vectors, not scalars), is computed. The similarity distance should reflect variations not only in magnitude but also in the preferences and behaviors induced by the reward functions. This is characterized by the property of policy invariance, which ensures that reward functions yielding the same optimal policies are considered similar even if their numerical reward values differ (Ng et al., 1999). This makes direct reward comparisons via distance measures such as Euclidean or Kullback-Leibler (KL) divergence unfavorable since these distances do not maintain policy invariance. To satisfy policy invariance, traditional reward comparison techniques have adopted indirect approaches, which compare behaviors derived from optimized policies generated from the reward functions under comparison (Arora & Doshi, 2021). However, these indirect approaches pose the following challenges: (1) they can be slow and resource-intensive due to policy learning via RL, and (2) policy learning might not be favorable in critical environments such as healthcare or autonomous vehicles, where safety considerations are important (Amodei et al., 2016; Thomas et al., 2021). Therefore, the development of direct reward comparison methods that bypass policy learning while maintaining policy invariance is highly important.

To achieve policy invariance in direct reward comparisons, Gleave et al. (2020) introduced the Equivalent Policy Invariant Comparison (EPIC) pseudometric. Given the task to compare two reward functions, EPIC first performs reward canonicalization to express the rewards in a standardized form by removing shaping; and then computes the Pearson distance to calculate the difference between the canonical reward functions. Although theoretically rigorous, EPIC falls short in practice since it is designed to compare reward functions under high transition coverage, when the majority of transitions within the space of explored states and actions, are sampled. In practical scenarios, this might be impractical due to transition sparsity—a condition where only a minority of transitions are sampled. This sparsity makes EPIC vulnerable to unsampled transitions, which can distort the computation of reward expectations in canonicalization (see Section 3.4). Transition sparsity can be attributed to: (1) **limited sampling** - when challenges in data collection result in few transitions being sampled; and (2) **feasibility constraints** - where environmental or agent-specific limitations restrict certain transitions. Consider, for instance, a standard 10×10 Gridworld domain where each (x, y) coordinate represents a state (see Figure 1). The total number of possible transitions is at least 10000 if one or more actions exist between any two states. However, feasibility constraints such as movement restrictions might significantly limit the transitions explored. For example, an agent that can only take

four single-step cardinal actions per given state will explore fewer than 400 transitions (see Figure 1c). To illustrate the impact of limited sampling, consider a scenario where transitions are sampled via policy rollouts (trajectory simulations from a given policy). In this scenario, the extent of sampled transitions is directly influenced by the frequency of policy rollouts. When the number of rollouts is low, fewer transitions will likely be sampled, and conversely, when the number of rollouts is high, a greater proportion of transitions is likely to be sampled (see Figure 1a and 1b).

Contributions In this paper, we introduce the Sparsity Agnostic Reward Distance (SARD) pseudometric, designed to improve reward comparisons in environments characterized by high transition sparsity. SARD demonstrates greater robustness compared to existing pseudometrics (such as EPIC), which assume reward samples with high transition coverage. SARD’s strength lies in its ability to integrate reward samples with diverse transition distributions, which are common in scenarios with low coverage. We provide a theoretical justification for SARD’s robustness and demonstrate its superiority through experiments in four domains of varying complexity: Gridworld, Bouncing Balls, Drone Combat, and a StarCraft 2 environment. For the simpler domains, Gridworld and Bouncing Balls, we evaluate SARD against manually defined factors such as nonlinear reward functions and feasibility constraints, to fully understand its strengths and limitations under controlled conditions. In the more complex domains, StarCraft 2 and Drone Combat, we assess SARD in battlefield scenarios characterized by large state and action spaces, to gauge how it will likely to perform in realistic settings. Our final experiment explores a novel and practical application of these pseudometrics as distance measures within a k-nearest neighbors algorithm, tailored to classify agent behaviors based on reward functions computed via IRL. Empirical results highlight SARD’s superior performance, evidenced by its ability to find higher similarity between rewards generated from the same agents and higher variation between rewards from different agents. These results emphasize the crucial need to accommodate transition sparsity in reward comparisons.

2 Related Works

The EPIC pseudometric is the first direct reward comparison technique that circumvents policy learning while maintaining policy invariance (Gleave et al., 2020). In practical settings, EPIC’s major limitation is that it is designed to compare rewards under high transition coverage. In scenarios characterized by transition sparsity, EPIC underperforms due to its high sensitivity to unsampled transitions, which can cause a distribution mismatch between sampled and expected transitions, distorting the computation of reward expectations (refer to Section 3.4). This limitation has been observed by Wulfe et al. (2022), who suggested the Dynamics-Aware Reward Distance (DARD) pseudometric. DARD improves on EPIC by considering transitions that are closer to being physically realizable; however, it remains sensitive to unsampled transitions, which limits its efficacy. Additionally, DARD requires access to transition models, which might be inaccessible or difficult to reliably estimate under transition sparsity.

Skalse et al. (2023) also introduced a family of reward comparison pseudometrics, known as Standardized Reward Comparisons (STARC). These pseudometrics are shown to induce lower and upper bounds on worst-case regret, implying that a small STARC difference between two reward functions corresponds to similar behaviors. Among the different STARC canonical forms explored, the Value-Adjusted Levelling (VAL) function is shown to have a higher correlation to regret compared to both EPIC and DARD. While an improvement, the major flaw with VAL is that it involves the estimation of value functions, which carry a significantly higher computational cost compared to both EPIC and DARD. To compute VAL in small environments, value iteration can be performed, which has polynomial complexity in terms of the state and action spaces (Skalse et al., 2023). For larger environments, value functions can be approximated via neural networks updated with on-policy Bellman updates (Skalse et al., 2023). Since the primary motivation for direct reward comparisons is to eliminate policy learning to lower computational costs, incorporating value functions in these pseudometrics is somewhat contradictory. Therefore, we do not consider VAL as a viable direct reward comparisons pseudometric.

The task of reward comparisons lies within the broader theme of reward evaluations, which aim to explain or interpret the relationship between rewards and agent behavior. Some notable works tackling this theme, include, Lambert et al. (2024), who developed benchmarks to evaluate reward models in Large Language

Models (LLMs), which are often trained using RL via human feedback (RLHF), to align with human values. These benchmarks assess criteria such as communication, safety and reasoning capabilities across a variety of reward models. In another line of work, Mahmud et al. (2023) presented a framework leveraging human explanations to evaluate and realign rewards for agents trained via IRL on limited data. Lastly, Russell & Santos (2019) proposed a method that examines the consistency between global and local explanations, to determine the extent to which a reward model captured complex agent behavior. Similar to reward comparisons, reward evaluations can be influenced by shaping functions, thus necessitating techniques such as canonicalization as preprocessing steps to eliminate shaping (Jenner & Gleave, 2022).

Reward shaping is a technique that transforms a base reward function into alternate forms (Ng et al., 1999). This technique is mainly employed in RL for reward design where heuristics and domain knowledge are integrated to accelerate learning (Mataric, 1994; Hu et al., 2020; Cheng et al., 2021; Gupta et al., 2022; Suay et al., 2016). Several applications of reward shaping have been explored, and some notable examples include: training autonomous robots for navigation (Tenorio-Gonzalez et al., 2010); training agents to ride bicycles (Randløv & Alstrøm, 1998); improving agent behavior in multiagent contexts such as the Prisoner’s Dilemma (Babes et al., 2008); and scaling RL algorithms in complex games (Lample & Chaplot, 2017; Christiano et al., 2017). Among several reward shaping techniques, potential-based shaping is the most popular due to its preservation of policy invariance, ensuring that the set of optimal policies remains unchanged between different versions of reward functions (Ng et al., 1999; Wiewiora et al., 2003; Gao & Toni, 2015).

3 Preliminaries

This section establishes the necessary foundation for understanding the task of direct reward comparisons. We review existing pseudometrics and discuss their limitations, which SARD aims to address.

3.1 Markov Decision Processes

A Markov Decision Process (MDP) is defined as a tuple $(\mathcal{S}, \mathcal{A}, \gamma, T, R)$, where \mathcal{S} and \mathcal{A} are the state and action spaces, respectively. The transition model $T : \mathcal{S} \times \mathcal{A} \times \mathcal{S} \rightarrow [0, 1]$, dictates the probability distribution of moving from one state, $s \in \mathcal{S}$, to another state, $s' \in \mathcal{S}$, under an action $a \in \mathcal{A}$, and each given transition is specified by the tuple (s, a, s') . The discount factor $\gamma \in [0, 1]$ reflects preference for immediate over future rewards. The reward function is denoted by $R : \mathcal{S} \times \mathcal{A} \times \mathcal{S} \rightarrow \mathbb{R}$, and for each transition, the reward is denoted by $R(s, a, s')$. The distributions over \mathcal{A} and \mathcal{S} are denoted by $\mathcal{D}_{\mathcal{A}}$ and $\mathcal{D}_{\mathcal{S}}$ respectively; and the corresponding sets of distributions are denoted by $\Delta\mathcal{A}$ and $\Delta\mathcal{S}$ respectively. A trajectory $\tau = \{(s_0, a_0), (s_1, a_1), \dots, (s_n)\}$, $n \in \mathbb{Z}^+$, is a sequence of states and actions, with a total return: $g(\tau) = \sum_{t=0}^{\infty} \gamma^t R(s_t, a_t, s_{t+1})$. The goal in an MDP is to find a policy $\pi : \mathcal{S} \times \mathcal{A} \rightarrow [0, 1]$ (often via RL) that maximizes the expected return $\mathbb{E}[g(\tau)]$. In some situations, the rewards of an MDP are unknown, and IRL can be used to compute the rewards given agent demonstrations (Abbeel & Ng, 2004; Ng & Russell, 2000; Wulfmeier et al., 2015).

3.2 Policy Invariance

Policy invariance is a condition where an optimal policy remains unchanged when a reward function is modified typically through shaping (Ng et al., 1999; Jenner et al., 2022). In reward comparisons, policy invariance is a key property to satisfy, since it ensures that equivalent rewards will yield the same optimal policies (Gleave et al., 2020). Formally, any shaped reward can be represented by the additive relationship: $R'(s, a, s') = R(s, a, s') + F(s, a, s')$, where $F(s, a, s')$ is a shaping function. Potential shaping guarantees policy invariance, and it takes the form: $F(s, a, s') = \gamma\phi(s') - \phi(s)$, where ϕ is a state potential function. A potentially-shaped reward function, R' , is thus represented as:

$$R'(s, a, s') = R(s, a, s') + \gamma\phi(s') - \phi(s). \quad (1)$$

where R is the original reward function. Reward functions R and R' can be deemed equivalent since they yield the same optimal policies.

To effectively compare reward functions that may differ in numerical values but are equivalent since they yield the same optimal policies, the use of *pseudometrics* is highly important. Let X be a set, with (x, y, z)

elements of X , and let $d : X \times X \rightarrow [0, \infty)$ define a pseudometric. This pseudometric adheres to the following axioms: (premetric) $d(x, x) = 0$ for all $x \in X$; (symmetry) $d(x, y) = d(y, x)$ for all $x, y \in X$; and (triangular inequality) $d(x, y) \leq d(x, z) + d(z, y)$ for all $x, y, z \in X$. Unlike a true metric, a pseudometric does not require that: $d(x, y) = 0 \implies x = y$, making it ideal for identifying equivalent reward functions that might have different numerical values.

3.3 Equivalent Policy Invariant Comparison (EPIC)

The EPIC pseudometric directly compares reward functions without computing policies, while maintaining policy invariance (Gleave et al., 2020). EPIC’s *reward comparison process* involves two steps: first, reward functions are canonicalized into a standard form without shaping; and second, a Pearson distance is computed to differentiate the canonical rewards. The following definitions, by Gleave et al. (2020), describe EPIC.

Definition 1. (*Canonically Shaped Reward*) Let $R : \mathcal{S} \times \mathcal{A} \times \mathcal{S} \rightarrow \mathbb{R}$ be a reward function. Given distributions $\mathcal{D}_\mathcal{S} \in \Delta\mathcal{S}$ and $\mathcal{D}_\mathcal{A} \in \Delta\mathcal{A}$ over states and actions respectively, let S and S' be random variables distributed as $\mathcal{D}_\mathcal{S}$ and A be distributed as $\mathcal{D}_\mathcal{A}$. The canonically shaped reward is:

$$C_{EPIC}(R)(s, a, s') = R(s, a, s') + \mathbb{E}[\gamma R(s', A, S') - R(s, A, S') - \gamma R(S, A, S')]. \quad (2)$$

Canonicalization expresses rewards in form free of shaping. Given a potentially shaped reward, $R'(s, a, s') = R(s, a, s') + \gamma\phi(s') - \phi(s)$, canonicalization yields: $C_{EPIC}(R')(s, a, s') = C_{EPIC}(R)(s, a, s') + \phi_{res}$, where $\phi_{res} = \gamma\mathbb{E}[\phi(S)] - \gamma\mathbb{E}[\phi(S')]$ is the remaining residual potential. EPIC assumes that S and S' are identically distributed such that $\mathbb{E}[\phi(S)] = \mathbb{E}[\phi(S')]$, which results in $\phi_{res} = 0$. This assumption leads to Proposition 1:

Proposition 1. (*The Canonically Shaped Reward is Invariant to Shaping*) Let $R : \mathcal{S} \times \mathcal{A} \times \mathcal{S} \rightarrow \mathbb{R}$ be a reward function, $\mathcal{D}_\mathcal{S} \in \Delta\mathcal{S}$ and $\mathcal{D}_\mathcal{A} \in \Delta\mathcal{A}$ be distributions over states and actions, $\phi : \mathcal{S} \rightarrow \mathbb{R}$ a state potential function, and $R'(s, a, s') = R(s, a, s') + \gamma\phi(s') - \phi(s)$ be the shaped reward. Then: $C_{EPIC}(R) = C_{EPIC}(R')$.

Proposition 1 means that reward functions R and R' , can be compared in their basis form, without the effect of shaping. Finally, the EPIC pseudometric between two reward functions, R_A and R_B , is computed as:

$$D_{EPIC}(R_A, R_B) = D_\rho(C_{EPIC}(R_A)(S, A, S'), C_{EPIC}(R_B)(S, A, S')), \quad (3)$$

where:

$$D_\rho(R_A, R_B) = \sqrt{1 - \rho(R_A, R_B)} / \sqrt{2}, \quad (4)$$

is the Pearson distance, and ρ is the Pearson correlation. The Pearson distance ensures that EPIC is scale and shift invariant, whilst canonicalization makes EPIC invariant to shaping (Gleave et al., 2020). Computing the exact expectation terms in EPIC is almost impractical because reward values are needed for all transitions. When a reward function has a large (or infinite) state or action space, the sample-based EPIC can be computed as follows:

Definition 2. (*Sample-based EPIC*) Given transition samples from a coverage distribution \mathcal{D} and a batch B_M of N_M samples from the joint state and action distributions. The canonically shaped reward is:

$$\begin{aligned} C_{EPIC}(R)(s, a, s') \approx & R(s, a, s') + \frac{\gamma}{N_M} \sum_{(x,u) \in B_M} R(s', u, x) - \frac{1}{N_M} \sum_{(x,u) \in B_M} R(s, u, x) \\ & - \frac{\gamma}{N_M^2} \sum_{(x,\cdot) \in B_M} \sum_{(x',u) \in B_M} R(x, u, x') \end{aligned} \quad (5)$$

3.4 Transition Undersampling

Consider a reward function $R : \mathcal{S} \times \mathcal{A} \times \mathcal{S}$, where \mathcal{S} is the state space and \mathcal{A} is the action space. Rewards are sampled from a coverage distribution, \mathcal{D} , which spans a state space $\mathcal{D}_\mathcal{S} \in \mathcal{S}$ and and action space $\mathcal{D}_\mathcal{A} \in \mathcal{A}$. This yields the set of possible transitions, $\mathcal{T}^\mathcal{D} = \mathcal{D}_\mathcal{S} \times \mathcal{D}_\mathcal{A} \times \mathcal{D}_\mathcal{S}$, where $\mathcal{T}^\mathcal{D} \subseteq \mathcal{S} \times \mathcal{A} \times \mathcal{S}$. Due to limited sampling and feasibility constraints, the transitions sampled in reality are represented by $\mathcal{T}^\mathcal{S} \subseteq \mathcal{T}^\mathcal{D}$, while

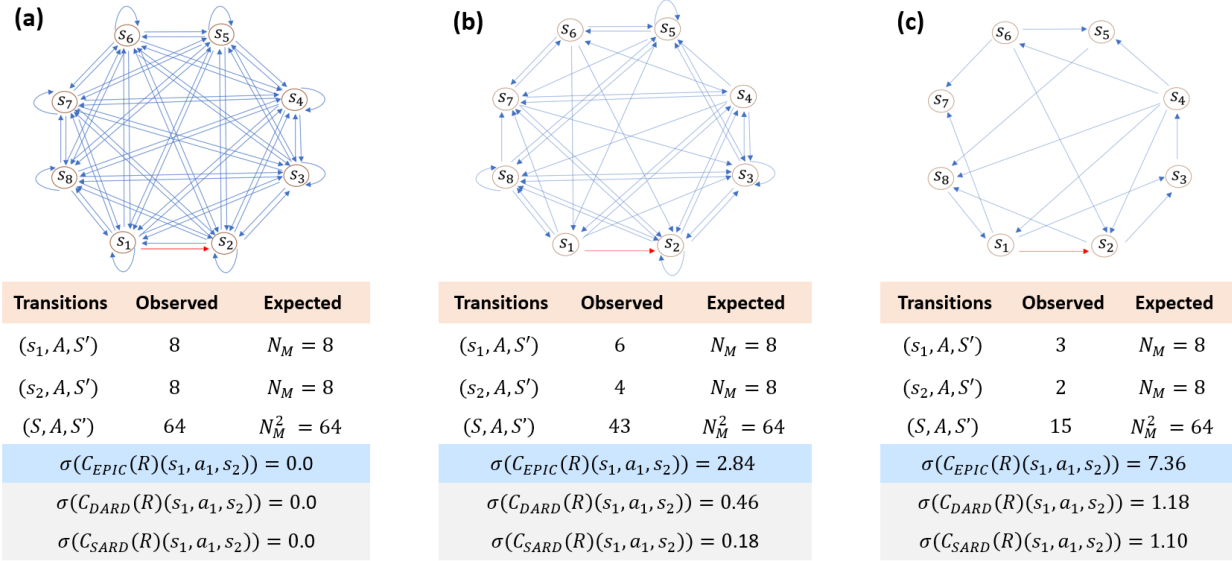


Figure 2: (Impact of transition undersampling in computing $C_{EPIC}(R)(s_1, a_1, s_2)$) Observed transitions are those explored in the reward sample, and expected transitions are those that EPIC anticipates, assuming full coverage. As coverage decreases from (a) to (c), the number of observed transitions relative to expected transitions decreases. Consequently, the standard deviation for $C_{EPIC}(R)(s_1, a, s_2)$ increases, indicating EPIC’s increased instability due to unsampled transitions. For comparison, the DARD and SARD estimates have lower standard deviations, signifying high stability under transition sparsity.

the unsampled transitions are denoted by $\mathcal{T}^U \subseteq \mathcal{T}^D$. A major limitation of pseudometrics such as EPIC (and to some extent, DARD), is that they are designed to compare reward functions under high transition coverage where, $|\mathcal{T}^S| \approx |\mathcal{T}^D|$. As $|\mathcal{T}^U| \rightarrow |\mathcal{T}^D|$, the performance of these pseudometrics significantly degrades due to transition undersampling.

To illustrate this in detail, consider Equation 5, used to approximate EPIC (Equation 2). To perform the computation, we need to estimate: $\mathbb{E}[R(s', A, S')]$ by dividing the sum of rewards from s' to S' by N_M transitions; $\mathbb{E}[R(s, A, S')]$ by dividing the sum of rewards from s to S' by N_M transitions; and $\mathbb{E}[R(S, A, S')]$ by dividing the sum of all rewards from S to S' by N_M^2 transitions, where $N_M = |\mathcal{D}_S \times \mathcal{D}_A|$. Every state $s \in S$ is expected to have N_M transitions to all other states S' , which is impractical under transition sparsity when a high number of transitions remain unsampled. Since reward summations are divided by large denominators N_M and N_M^2 (see Equation 5), when coverage is low, the number of sampled transitions needed to estimate the reward expectation terms will be fewer than expected, introducing significant error. Moreover, to eliminate residual shaping, $\phi_{res} = \gamma \mathbb{E}[\phi(S)] - \gamma \mathbb{E}[\phi(S')]$, EPIC assumes that S and S' are identically distributed, which favors reward samples with high transition coverage where each state likely has a transition to every other state.

Figure 2 illustrates an example showing the effect of transition undersampling on computing EPIC, across three reward samples spanning a state space $S = S' = \{s_1, \dots, s_8\}$, and an action space, $A = \{a_1\}$, such that $N_M = 8$, under different levels of transition sparsity. Rewards are defined as $R(s_i, a_1, s_j) = 1 + \gamma \phi(s_j) - \phi(s_i)$, where $i, j \in \{1, \dots, 8\}$, and state potentials are randomly generated and constrained to: $|\phi(s)| \leq 20$, with $\gamma = 0.5$. The task is to compute $C_{EPIC}(R)(s_1, a_1, s_2)$ over 1000 simulations. For all reward samples, the mean $\mu(C_{EPIC}(R)(s_1, a_1, s_2)) \approx 0$, but the standard deviation, $\sigma(C_{EPIC}(R)(s_1, a_1, s_2))$ varies based on coverage. In Figure 2a, the reward sample has high coverage (100%), hence, the number of observed and expected transitions are equal. In this scenario, EPIC is highly effective such that all shaped rewards are mapped to the same value (≈ 0), resulting in a standard deviation $\sigma(C_{EPIC}(R)(s_1, a_1, s_2)) = 0$, which highlights consistent reward canonicalization. In Figure 2b, the reward sample has moderate coverage, ($\approx 67\%$), and observed transitions are undersampled relative to expected transitions. As a result, $\sigma(C_{EPIC}(R)(s_1, a_1, s_2)) = 2.84$, which is relatively high, signifying EPIC’s sensitivity to undersampling. In Figure 2c, the reward sample

exhibits low coverage ($\approx 23\%$), leading to a significant discrepancy between the number of observed and expected transitions. Consequently, $\sigma(C_{EPIC}(R)(s_1, a_1, s_2)) = 7.36$, indicating EPIC’s increased instability due to transition undersampling. For comparison, we have added the DARD and SARD estimates, and we can see that these distances have lower standard deviations, signifying greater stability.

EPIC’s limitations have also been acknowledged by Wulfe et al. (2022), who propose DARD, to only consider transitions that are closer to being physically realizable. The DARD pseudometric is given by:

$$C_{DARD}(R)(s, a, s') = R(s, a, s') + \mathbb{E}[\gamma R(s', A, S'') - R(s, A, S') - \gamma R(S', A, S'')],$$

where $A \sim \mathcal{D}_A$, $S' \sim T(s, A)$, $S'' \sim T(s', A)$, and T is the transition model. DARD is invariant to shaping and generally improves upon EPIC by eliminating the identical distribution assumption and by separating the states connected from s (denoted by S') and s' (denoted by S''). However, DARD still suffers from undersampling since it requires transitions from S' to S'' , which may not exist. Furthermore, DARD requires access to the transition model, which might be inaccessible or unreliable to estimate under transition sparsity. These factors make DARD a modest improvement over EPIC, but it still struggles to compare reward functions under high transition sparsity. This paper uses DARD as an experimental baseline.

4 Approach: Sparsity Agnostic Reward Distance (SARD)

Our motivation in SARD is to develop a direct reward comparison technique that minimizes assumptions on the structure and distribution of reward samples, ensuring robustness under high transition sparsity. To derive SARD, we first modify C_{EPIC} (Equation 2) to eradicate the need for high transition coverage. This is achieved by eliminating the assumption that S and S' are identically distributed; and ensuring that reward expectations computed for transitions from s , s' and S are different. This approach reduces transition undersampling, since reward expectations are computed based on the observed distribution of sampled transitions. With these considerations, the modified canonical equation becomes:

$$C_1(R)(s, a, s') = R(s, a, s') + \mathbb{E}[\gamma R(s', A, S_1) - R(s, A, S_2) - \gamma R(S_3, A, S_4)], \quad (6)$$

where the random variables: S_1 and S_2 are subsequent states to s' and s , respectively; S_3 encompasses all initial states for all sampled transitions; and S_4 are subsequent states to S_3 . Applying C_1 to a shaped reward $R'(s, a, s') = R(s, a, s') + \gamma\phi(s') - \phi(s)$, we get:

$$C_1(R')(s, a, s') = C_1(R)(s, a, s') + \phi_{res1}, \quad (7)$$

where,

$$\phi_{res1} = \mathbb{E}[\gamma^2\phi(S_1) - \gamma^2\phi(S_4) + \gamma\phi(S_3) - \gamma\phi(S_2)]. \quad (8)$$

C_1 is not theoretically robust since its prone to shaping due to residual potential ϕ_{res1} . To cancel $\mathbb{E}[\phi(S_i)]$, $\forall i \in \{1, \dots, 4\}$, we can add rewards $R(S_i, A, k_i)$ to induce potentials $\gamma\phi(k_i) - \phi(S_i)$; where k_i can be any arbitrary distribution of states. This results in the equation:

$$\begin{aligned} C_2(R)(s, a, s') &= R(s, a, s') + \mathbb{E}[\gamma R(s', A, S_1) - R(s, A, S_2) - \gamma R(S_3, A, S_4) \\ &\quad + \gamma^2 R(S_1, A, k_1) - \gamma R(S_2, A, k_2) + \gamma R(S_3, A, k_3) - \gamma^2 R(S_4, A, k_4)]. \end{aligned} \quad (9)$$

Applying C_2 to shaped reward $R'(s, a, s') = R(s, a, s') + \gamma\phi(s') - \phi(s)$, we get:

$$C_2(R')(s, a, s') = C_2(R)(s, a, s') + \phi_{res2}, \quad (10)$$

where,

$$\phi_{res2} = \mathbb{E}[\gamma^3\phi(k_1) - \gamma^3\phi(k_4) + \gamma^2\phi(k_3) - \gamma^2\phi(k_2)]. \quad (11)$$

(See Appendix A.5 for derivations of ϕ_{res1} and ϕ_{res2}). The canonical form C_2 is preferable to C_1 , since it enables the selection of k_i to eradicate ϕ_{res2} . A convenient solution is to ensure that: $k_1 = k_4$ and $k_2 = k_3$ such that $\mathbb{E}[\phi(k_1)] = \mathbb{E}[\phi(k_4)]$ and $\mathbb{E}[\phi(k_2)] = \mathbb{E}[\phi(k_3)] \implies \phi_{res2} = 0$. We choose the solution: $k_1 = k_4 = S_5$, and $k_2 = k_3 = S_6$; where S_5 are states subsequent to S_1 , and S_6 are states subsequent to S_2 . This leads to the following SARD definition:

Definition 3. (*Sparsity Agnostic Canonically Shaped Reward*) Let $R : \mathcal{S} \times \mathcal{A} \times \mathcal{S} \rightarrow \mathbb{R}$ be a reward function. Given distributions $\mathcal{D}_S \in \Delta(\mathcal{S})$ and $\mathcal{D}_A \in \Delta(\mathcal{A})$ over states and actions respectively, let $\{S_1, \dots, S_6\}$ be random variables distributed such that: S_1 and S_2 are subsequent states to s' and s , respectively; S_3 encompasses all initial states from all sampled transitions; S_4 , S_5 , and S_6 are subsequent states to S_3 , S_1 and S_2 , respectively. The Sparsity Agnostic Canonically Shaped Reward is defined as:

$$C_{SARD}(R)(s, a, s') = R(s, a, s') + \mathbb{E}[\gamma R(s', A, S_1) - R(s, A, S_2) - \gamma R(S_3, A, S_4) + \gamma^2 R(S_1, A, S_5) - \gamma R(S_2, A, S_6) + \gamma R(S_3, A, S_6) - \gamma^2 R(S_4, A, S_5)]. \quad (12)$$

The choices for k_i in C_{SARD} (Equation 12), S_5 and S_6 , are ideal for two reasons: First, for any reward sample, we are guaranteed to compute reliable expectation estimates for the first six terms, since for each set of transitions (S_i to S_j), S_j is created based on S_i ; hence, these transitions naturally align with any reward sample distribution. However, for transitions in the last two terms, (S_3 to S_6) and (S_4 to S_5), S_6 and S_5 , are not directly created based on S_3 and S_4 , as they were previously defined for S_2 and S_1 ; therefore, these terms are susceptible to transition undersampling, since they might require transitions not present in the reward sample. Second, while there might be unsampled transitions from (S_4 to S_5), and (S_3 to S_6), a minimal set of sampled transitions is likely to exist, because:

- Transitions $(S_1, A, S_5) \subseteq (S_4, A, S_5)$, since S_1 are subsequent states to s' , and S_4 are subsequent states for all sampled transitions, hence, $(S_1 \subseteq S_4)$.
- With the exception of terminal states in S_2 , transitions $(S_2, A, S_6) \subseteq (S_3, A, S_6)$, since every state in S_2 becomes an initial state for some sampled transition, and S_3 encompasses all initial states, hence, $(S_2 \subseteq S_3)$.

Therefore, we are likely to get decent reward expectation estimates for the transitions: (S_3 to S_6) and (S_4 to S_5). These factors ensure that the upper bound residual potential for C_{SARD} is lower than that of C_1 —which we treat as a modified version of EPIC adapted to work in environments that might not have high transition coverage (refer to Equation 6). This leads to Theorem 1:

Theorem 1. Assuming that the transitions (S_1 to S_5) and (S_2 to S_6) are non-empty, the upper bound residual potential for $C_{SARD}(R)(s, a, s')$ is lower than that of $C_1(R)(s, a, s')$.

Proof. See Appendix A.1.

In extremely rare instances when both (S_1 to S_5) and (S_2 to S_6) are empty, the upper bound residual potential for $C_{SARD}(R)(s, a, s')$ will be similar to that of $C_1(R)(s, a, s')$. SARD canonicalization is also invariant to shaping, as described by Proposition 2.

Proposition 2. (*The Sparsity Agnostic Canonically Shaped Reward is Invariant to Shaping*) Let $R : \mathcal{S} \times \mathcal{A} \times \mathcal{S} \rightarrow \mathbb{R}$ be a reward function, $\phi : \mathcal{S} \rightarrow \mathbb{R}$, a state potential function. Given a shaped reward $R'(s, a, s') = R(s, a, s') + \gamma\phi(s') - \phi(s)$:

$$C_{SARD}(R) = C_{SARD}(R').$$

Proof. See Appendix A.2.

Finally, given rewards R_A and R_B , the SARD pseudometric is computed as follows:

$$D_{SARD}(R_A, R_B) = D_p(C_{SARD}(R_A)(S, A, S'), C_{SARD}(R_B)(S, A, S')), \quad (13)$$

where, D_p is the Pearson distance (see Equation 4). In summary, SARD is designed to improve reward comparisons under transition sparsity. To achieve this, SARD eliminates the assumption that S and S' are identically distributed, and also reduces the impact of transition undersampling, by canonicalizing rewards solely based on sampled transitions. A challenge with SARD, however, is its computational cost relative to EPIC, though it is comparable to DARD. To canonicalize all transitions in a reward sample with N_T transitions, the computational costs for EPIC, DARD, and SARD $\approx O(N_T)$, $O(N_T^2)$ and $O(N_T^2)$, respectively

(see Appendix A.9). A sample-based approximation for SARD is provided in Appendix A.3, and Appendix A.4 presents a generalized formula for possible SARD extensions. In Appendix A.8, we establish an upper bound for regret in terms of the SARD pseudometric, showing that when $D_{SARD} \rightarrow 0$, the difference between the policies induced by the reward functions under comparison is close to 0.

5 Experiments

To evaluate SARD, we examine the following hypotheses:

H1: SARD is a reliable reward comparison pseudometric under high transition sparsity.

H2: SARD can enhance the task of classifying agent behaviors based on their reward functions.

In these hypotheses, we compare the performance of SARD to both EPIC and DARD using sample-based approximations. In **H1**, we analyze SARD’s robustness under transition sparsity resulting from limited sampling and feasibility constraints. In **H2**, we investigate a practical use case to classify agent behaviors using their reward functions. Experiment 1 tests **H1** and Experiment 2 tests **H2**.

Domain Specifications To conduct Experiment 1, we need the capability to vary the number of sampled transitions, since the goal is to test SARD’s performance under different levels of transition sparsity. Therefore, Experiment 1 is performed in the Gridworld and Bouncing Balls domains, as they provide the flexibility for parameter variation to control the size of the state and action spaces². These two domains have also been studied in the EPIC and DARD papers, respectively. The Gridworld domain simulates agent movement from a given initial state to a specified terminal state under a static policy. States are defined by (x, y) coordinates where $0 \leq x < N$ and $0 \leq y < M$ implying $|\mathcal{S}| = NM$. The action space consists of four cardinal directions (single steps), and the environment is stochastic, with a probability ϵ of transitioning to any random state irrespective of the selected action. When $\epsilon = 0$, a feasibility constraint is imposed, preventing the agent from making random transitions. The Bouncing Balls domain, adapted from (Wulfe et al., 2022), simulates a ball’s motion from a starting state to a target state while avoiding randomly mobile obstacles. These obstacles add complexity to the environment since the ball might need to change its strategy to avoid obstacles (at a distance, $d = 3$). Each state is defined by the tuple (x, y, d) , where (x, y) indicates the ball’s current location, and d indicates the ball’s Euclidean distance to the nearest obstacle, such that: $0 \leq x < N$, $0 \leq y < M$, and $d \leq \max(M, N)$. The action space includes eight directions (cardinals and ordinals), we also define the stochasticity-level parameter ϵ for choosing random transitions.

For Experiment 2, the objective is to test SARD’s performance in near-realistic domain settings, where we have no control over factors such as the nature of rewards and the level of transition sparsity. Therefore, for domain settings, in addition to the Gridworld and the Bouncing Balls domains with the setup similar to Experiment 1 but fixed parameters, we also examine the StarCraft 2 and Drone Combat domains which both simulate battlefield environments where a controlled multiagent team aims to defeat a default AI enemy team (Anurag, 2019; Vinyals et al., 2019). These domains resemble complex scenarios with large state and action spaces (almost infinite for Starcraft2), enabling us to test SARD’s (as well as the other pseudometrics) generalization to near-realistic scenarios. Additional details about these domains, including information about the state and action features are described in Appendix C.1.

Reward Functions Extrinsic reward functions are manually defined using a combination of state and action features. For the Starcraft2 and Drone Combat domains, we use the default game engine scores (also based on state and action features), as the reward function (see Appendix B.1). For the Gridworld and Bouncing Balls domains, in each reward function, the reward value $R(s, a, s')$ is derived from the decomposition of state and action features, where, (s_{f1}, \dots, s_{fn}) is from the starting state s ; (a_{f1}, \dots, a_{fm}) is from the action a ; and $(s'_{f1}, \dots, s'_{fn})$ is from the subsequent state s' . For the Gridworld domain, these features are the (x, y) coordinates, and for the Bouncing Balls domain, these include (x, y, d) , where d is the distance of the obstacle nearest to the ball. For each unique transition, using randomly generated

²Experiment 1 excludes the Drone Combat and StarCraft 2 environments because these domains have very large state and action spaces that hinder effective coverage computation.

constants: $\{u_1, \dots, u_n\}$ for incoming state features; $\{w_1, \dots, w_m\}$ for action features; $\{v_1, \dots, v_n\}$ for subsequent state features, we create polynomial and random rewards as follows:

Polynomial: $R(s, a, s') = u_1 s_{f1}^\alpha + \dots + u_n s_{fn}^\alpha + w_1 a_{f1}^\alpha + \dots + w_m a_{fm}^\alpha + v_1 s'_{f1}^\alpha + \dots + v_n s'_{fn}^\alpha$,
 where α is randomly generated from 1-10, denoting the degree of the polynomial.

Random: $R(s, a, s') = \beta$,
 where β is a randomly generated reward for each unique transition.

For the polynomial rewards, α is the same across the entire sample, but other constants vary between different transitions. The same reward relationships are used to model potential shaping functions. In addition, we also explore linear and sinusoidal reward models as described in Appendix B.1.

For complex environments such as Starcraft2 and the Drone Combat domain, specifying reward functions can be challenging, hence we also incorporate IRL to infer rewards from demonstrated behavior. For our experiments, we consider the following IRL rewards: Maximum Entropy IRL (Maxent) (Ziebart et al., 2008); Adversarial IRL (AIRL) (Fu et al., 2018); and Preferential-Trajectory IRL (PTIRL) (Santos et al., 2021). The full descriptions for these algorithms is described in Appendix C.3.

5.1 Experiment 1: Transition Sparsity

Objective: The goal of this experiment is to test SARD’s ability to identify similar reward samples under transition sparsity as a result of limited sampling and feasibility constraints.

Relevance: The EPIC pseudometric struggles under high transition sparsity since it is designed to compare reward functions (as well as samples), under high coverage. SARD is developed to overcome EPIC’s limitations, and this experiment tests SARD’s performance relative to EPIC and DARD, on varying levels of transition coverage due to feasibility constraints and limited sampling.

Approach: This experiment is conducted on a 20×20 Gridworld domain and a 20×20 Bouncing Balls domain. For all simulations, manual rewards are used since they enable the flexibility to vary the nature of the relationship between reward values and features, enabling us to test the performance of the pseudometrics on diverse reward values, which include polynomial and random reward relationships. We also vary the shaping potentials such that $|R(s, a, s')| \leq |\gamma\phi(s') - \phi(s)| \leq 5|R(s, a, s')|$.

For each domain, a ground truth reward function (GT) and an equivalent potentially shaped reward function (SH) are generated, both with full coverage (100%). Using rollouts from a uniform policy, rewards R and R' are sampled from GT and SH respectively, and they might differ in transition composition. After sample generation, R and R' are canonicalized and reward distances are computed using common transitions between them, under varying levels of coverage (to test limited sampling) and feasibility constraints. The SARD, DARD, and EPIC reward distances are computed, as well as DIRECT, which is the Pearson distance of rewards without canonicalization. Since R and R' are drawn from equivalent reward functions, an accurate pseudometric should yield distances close to the minimum Pearson distance, $D_\rho = 0$; and the least accurate should yield a distance close to the maximum, $D_\rho = 1$. DIRECT serves as a worst-case performance baseline, since it computes reward distances without canonicalization (needed to remove shaping). We perform 200 simulation trials for each comparison task, and record the mean reward distances.

Simulations and Results: Limited Sampling: Using rollouts from a uniform policy, we sample R and R' from GT and SH , respectively, under a stochasticity-level parameter, $\epsilon = 0.1$. The number of transitions sampled is controlled by varying the number of policy rollouts (rollout counts) from 1 up to 500. The corresponding coverage is computed as the number of sampled transitions over the possible number of transitions ($= |\mathcal{S} \times \mathcal{A} \times \mathcal{S}|$). Figure 3a summarizes the variation of reward distances to transition coverage due to different levels of transition sampling in the Gridworld, and Bouncing Balls domains. As shown, SARD generally outperforms other baselines since it converges towards $D_\rho = 0$ faster, even when coverage is low. DARD generally outperforms EPIC; however, it’s highly prone to shaping compared to SARD since it’s more sensitive to unsampled transitions. All pseudometrics generally outperform DIRECT, illustrating the

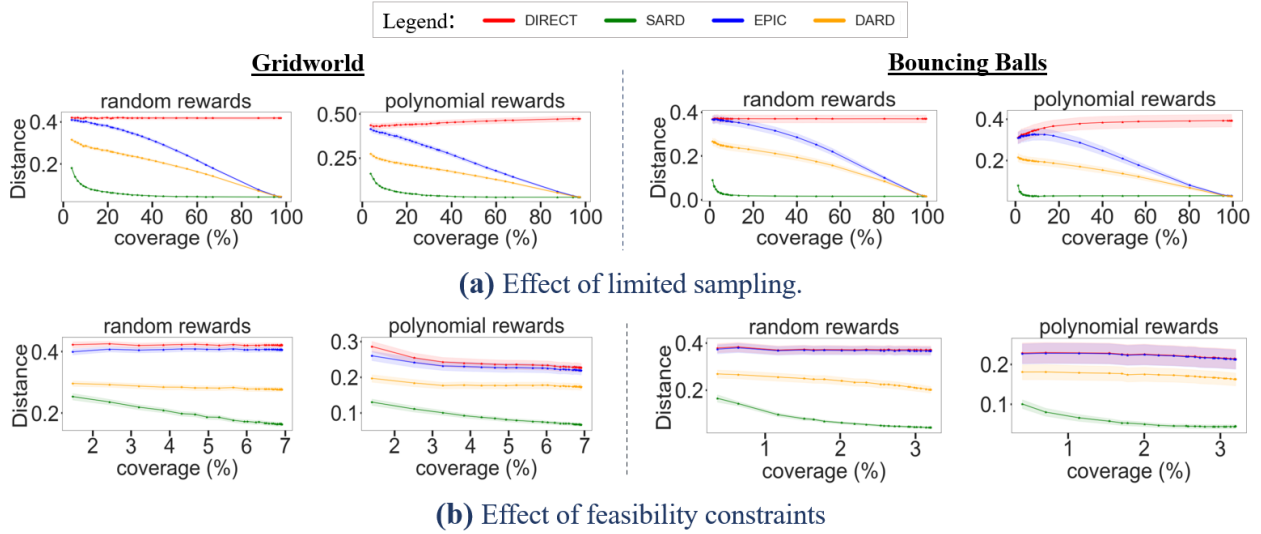


Figure 3: (Transition Sparsity) In both experiments, transition coverage is controlled by varying the number of policy rollouts from 1 to 500. In (a) EPIC and DARD lag behind SARD when transition coverage is low due to limited sampling from lower rollout counts, but gradually improves as transition coverage increases due to higher rollout counts. In (b), movement restrictions significantly lowers transition coverage, irrespective of the rollout sampling frequency, which negatively impacts EPIC’s performance.

value of removing shaping via canonicalization. No significant difference in the general trends of results are observed between the two domains, and additional simulations are presented in Appendix B. In conclusion, the proposed SARD consistently outperforms both EPIC and DARD, especially under limited sampling when coverage is low.

Simulations and Results: Feasibility Constraints: Using rollouts (similar range from 1 to 500) from a uniform policy, we sample R and R' from GT and SH , respectively. To impose feasibility constraints, we set the stochasticity-level parameter, $\epsilon = 0$, to restrict random transitions between states such that only movement to adjacent states is permitted. Figure 3b summarizes the results for the variation of reward distances to transition coverage under the movement restrictions. As shown, SARD significantly outperforms all the baselines. The movement restriction ensures that coverage is generally low ($< 10\%$), even though the number of rollouts is similar to those in the first experiment. DARD still outperforms EPIC, which performs relatively similar to DIRECT, indicating EPIC’s degraded performance under feasibility constraints.

5.2 Experiment 2: Classifying Agent Behaviors

Objective: The goal of this experiment is to assess SARD’s effectiveness as a distance measure in classifying agent behaviors based on their reward functions. If SARD is robust, it should identify similarities among reward functions from the same agents while differentiating reward functions from distinct agents.

Relevance: This experiment³ demonstrates a practical use-case for incorporating reward comparison pseudometrics to interpret reward functions by relating them to agent behavior. In many real-world situations, samples of agent behaviors are available, and there is a need to interpret the characteristics of the agents that produced these behaviors. For example, several works have attempted to predict player rankings and strategies using past game histories (Luo et al., 2020; Liu & Schulte, 2018; Yanai et al., 2022). This exper-

³Experiment 2 is related to prior works, Gleave et al. (2020) and Wulfe et al. (2022), where reward distances are computed for the ground truth, regressed, and IRL-generated reward types. Their results show that distances from each reward type are relatively similar, reflecting some form of reward grouping or clustering. However, these works do not explore real-world use-cases of this ‘reward grouping’ phenomenon, and our work presents a k-NN classification algorithm that utilizes reward distance similarity (between reward sample vectors) to classify agent behaviors, without the need for additional reward preprocessing.

iment takes a similar direction by attempting to classify the identities of agents from their unlabeled past trajectories using reward functions. The reliance on rewards rather than the original trajectories is based on the premise that reward functions are "succinct" and "robust", hence a preferable means to interpret agent behavior (Abbeel & Ng, 2004; Michaud et al., 2020).

Approach: In this experiment, we train a k -nearest neighbors (k -NN) classifier to classify unlabeled agent trajectories by indirectly using computed rewards, to identify the agents that produced these trajectories. We examine the k -NN algorithm since it is one of the most popular distance-based classification techniques. The experiment is conducted across all domains, and since we want to maximize classification accuracy, we consider different IRL rewards, including: Maxent, AIRL, PTIRL as well as manual (extrinsic) rewards. For manual rewards, we utilize the default game score for the Starcraft2 and Drone Combat domains, and polynomial rewards for the Gridworld and Bouncing Balls domains, where we induce random potential shaping. For each domain, we examine SARD, DIRECT, EPIC, and DARD as distance measures for a k -NN reward classification task. The steps for the approach are as follows:

1. Create agents $X = \{x_1, \dots, x_m\}$ with distinct behaviors.
2. For each agent, $x_i \in X$, generate trajectories $\{\tau_1^{x_i}, \dots, \tau_p^{x_i}\}$; and compute reward functions $\{R_1^{x_i}, \dots, R_p^{x_i}\}$ using IRL or manual specification.
3. Randomly shuffle all the computed reward functions \mathcal{R} (from all agents), and split into the training \mathcal{R}_{train} and testing \mathcal{R}_{test} sets.
4. Use each reward pseudometric as a distance measure to train a k -NN classifier with \mathcal{R}_{train} and test it with \mathcal{R}_{test} .

In step 1, different agent behaviors are controlled by varying the agents' policies (see Appendix C.2). In step 4, to train the classifier, grid-search is used to identify candidate values for k and γ , and twofold cross-validation (using \mathcal{R}_{train}) is used to optimize hyper-parameters based on accuracy. Since we assume potential shaping, the value of γ is unknown, hence its a hyper-parameter. To classify an arbitrary reward function $R_i \in \mathcal{R}_{test}$, we traverse reward functions $R_j \in \mathcal{R}_{train}$, and compute the distance, $D_\rho(R_i, R_j)$ using the reward pseudometrics. We then identify the top k -closest rewards to R_i , and choose the label of the most frequent class. We select a training to test set ratio of 70 : 30, and repeat this experiment 200 times.

Simulations and Results: Table 1 summarizes experimental results. As shown, SARD generally achieves higher accuracy compared to DIRECT, EPIC and DARD across all domains, indicating SARD effectiveness at discerning similarities between rewards produced by the same agents, and differences between those generated by different agents. This trend is more pronounced with manual rewards where SARD significantly outperforms other baselines. This can be attributed to potential shaping, which is intentionally induced in manual rewards that SARD is specialized to tackle. Therefore, SARD proves to be a more effective distance measure at classifying rewards subjected to potential shaping. For IRL-based rewards such as Maxent, AIRL, and PTIRL, while we assume potential shaping, non-potential shaping could be present. This explains the reduction in SARD's performance gap over EPIC and DARD, as well as the few instances where EPIC and DARD outperform SARD, though SARD is still generally dominant. Overall, SARD, EPIC, and DARD outperform DIRECT, emphasizing the importance of canonicalization at reducing the impact of shaping.

To verify the validity of results, Welch's t-tests for unequal variances are conducted across all domain and reward type combinations, to test the null hypotheses: (1) $\mu_{SARD} \leq \mu_{DIRECT}$, (2) $\mu_{SARD} \leq \mu_{EPIC}$, and (3) $\mu_{SARD} \leq \mu_{DARD}$; against the alternative: (1) $\mu_{SARD} > \mu_{DIRECT}$, (2) $\mu_{SARD} > \mu_{EPIC}$, and (3) $\mu_{SARD} > \mu_{DARD}$, where μ represents the sample mean. We reject the null when the p-value < 0.05 (level of significance), and conclude that: (1) $\mu_{SARD} > \mu_{DIRECT}$ for all instances; (2) $\mu_{SARD} > \mu_{EPIC}$ for 11 out of 12 instances, and (3) $\mu_{SARD} > \mu_{DARD}$ for 10 out of 12 instances. These tests are performed assuming normality as per central limit theorem, since the number of trials is 200. For additional details about the tests and accuracy metrics such as F1-scores, refer to Appendix C. In summary, we conclude that SARD is a more effective distance measure for classifying reward samples compared to its baselines.

Table 1: The accuracy (%) of different reward comparison distances in k -NN reward classification.

DOMAIN	REWARDS	DIRECT	EPIC	DARD	SARD
Gridworld	Manual	69.8	69.3	70.0	75.8
	Maxent	57.4	57.5	68.9	70.0
	AIRL	82.3	84.9	85.0	86.2
	PTIRL	82.2	84.2	83.4	86.0
Bouncing Balls	Manual	46.5	47.3	52.0	55.2
	Maxent	39.7	46.0	50.8	49.9
	AIRL	41.2	46.1	49.8	56.3
	PTIRL	70.3	71.1	69.5	72.4
Drone Combat	Manual	67.1	67.2	66.2	73.9
	Maxent	70.3	77.7	73.2	76.7
	AIRL	90.1	90.7	92.3	93.8
	PTIRL	52.5	63.7	65.1	78.3
StarCraft 2	Manual	65.5	67.4	69.5	76.5
	Maxent	72.3	74.1	73.9	74.8
	AIRL	75.1	75.3	78.1	77.0
	PTIRL	77.2	78.1	77.6	79.8

6 Conclusion and Future Work

This paper introduces SARD, a reward comparison pseudometric designed to address transition sparsity, a significant challenge encountered when comparing reward functions without high transition coverage. Conducted experiments demonstrate SARD’s superiority over state-of-the-art pseudometrics, such as EPIC and DARD, under limited sampling and feasibility constraints. Additionally, SARD proves effective as a distance measure for k -NN classification using reward functions to represent agent behavior. This implies that SARD can find higher similarities between reward functions generated by the same agent and higher differences between reward functions that are generated from different agents.

Most existing studies, including ours, have primarily focused on potential shaping, as it is the only additive shaping technique that guarantees policy invariance (Ng et al., 1999; Jenner et al., 2022). Future research should consider the effects of non-potential shaping on SARD (see Appendix B.5) or random perturbations, as these might distort reward functions that would otherwise be similar. This could help to standardize and preprocess a wider range of rewards that might not necessarily be potentially shaped. In computing reward distances, the Pearson distance is employed for its shift and scale invariance properties. However, this distance measure is highly sensitive to outliers, especially in the case of small reward samples. Future work should explore modifications such as Winsorization to mitigate the impact of outliers. Future studies should also explore applications of reward distance comparisons in scaling reward evaluations in IRL algorithms. For example, iterative IRL approaches such as MaxentIRL, often perform policy evaluations to assess the quality of the updated reward in each training trial. Integrating direct reward comparison pseudometrics to determine if rewards are converging, could help to skip the policy evaluation steps, thereby speeding up IRL. Finally, the development of reward comparison metrics has primarily aimed to satisfy policy invariance. A promising area to examine in the future is multicriteria policy invariance, where invariance might be conditioned to different criteria. For example, in the context of reward functions in Large Language Models (LLMs), it might be important to compute reward distance pseudometrics that consider different criteria such as bias, safety, or reasoning, to advance interpretability, which could be beneficial for applications such as reward fine-tuning and evaluation (Lambert et al., 2024).

References

Pieter Abbeel and Andrew Y Ng. Apprenticeship Learning via Inverse Reinforcement Learning. In *Proceedings of the Twenty-First International Conference on Machine Learning*, pp. 1, 2004.

- Dario Amodei, Chris Olah, Jacob Steinhardt, Paul Christiano, John Schulman, and Dan Mané. Concrete problems in ai safety. *arXiv preprint arXiv:1606.06565*, 2016.
- Koul Anurag. Ma-gym: Collection of Multi-agent Environments based on OpenAI gym. <https://github.com/koulanurag/ma-gym>, 2019.
- Saurabh Arora and Prashant Doshi. A Survey of Inverse Reinforcement Learning: Challenges, Method and Progress. *Artificial Intelligence*, 297(1), 2021.
- Monica Babes, Enrique Munoz de Cote, and Michael Littman. Social Reward Shaping in the Prisoner’s Dilemma (Short Paper). In *Proc. of 7th Int. Conf. on Autonomous Agents and Multiagent Systems (AAMAS)*, 2008.
- Ching-An Cheng, Andrey Kolobov, and Adith Swaminathan. Heuristic-guided Reinforcement Learning. In *Advances in Neural Information Processing Systems*, volume 34, 2021.
- Paul Christiano, Jan Leike, Tom B. Brown, Miljan Martic, Shane Legg, and Dario Amodei. Deep Reinforcement Learning from Human Preferences. *Advances in Neural Information Processing Systems*, 30, 2017.
- Chelsea Finn, Sergey Levine, and Pieter Abbeel. Guided Cost Learning: Deep Inverse Optimal Control via Policy Optimization. In *International Conference on Machine Learning*, pp. 49–58, 2016.
- Justin Fu, Katie Luo, and Sergey Levine. Learning Robust Rewards with Adversarial Inverse Reinforcement Learning. In *International Conference on Learning Representations*, 2018.
- Yang Gao and Francesca Toni. Potential Based Reward Shaping for Hierarchical Reinforcement Learning. In *Twenty-Fourth International Joint Conference on Artificial Intelligence*, 2015.
- Adam Gleave, Michael Dennis, Shane Legg, Stuart Russell, and Jan Leike. Quantifying Differences In Reward Functions. In *International Conference on Learning Representations*, 2020.
- Adam Gleave, Mohammad Taufeque, Juan Rocamonde, Erik Jenner, Steven Wang, Sam Toyer, Maximilian Ernestus, Nora Belrose, Scott Emmons, and Stuart Russell. Imitation: Clean imitation learning implementations. arXiv:2211.11972v1 [cs.LG], 2022. URL <https://arxiv.org/abs/2211.11972>.
- Abhishek Gupta, Aldo Pacchiano, Yuxiang Zhai, Sham Kakade, and Sergey Levine. Unpacking Reward Shaping: Understanding the Benefits of Reward Engineering on Sample Complexity. In *Advances in Neural Information Processing Systems*, volume 35, 2022.
- Yujing Hu, Weixun Wang, Hangtian Jia, Yixiang Wang, Yingfeng Chen, Jianye Hao, Feng Wu, and Changjie Fan. Learning to Utilize Shaping Rewards: A New Approach of Reward Shaping. In *Advances in Neural Information Processing Systems*, volume 33, 2020.
- Erik Jenner and Adam Gleave. Preprocessing Reward Functions for Interpretability. preprint arXiv:2203.13553, 2022.
- Erik Jenner, Herke van Hoof, , and Adam Gleave. Calculus on MDPs: Potential Shaping as a Gradient. preprint arXiv:2208.09570, 2022.
- Nathan Lambert, Valentina Pyatkin, Jacob Morrison, LJ Miranda, Bill Yuchen Lin, Khyathi Chandu, Nouha Dziri, Sachin Kumar, Tom Zick, Yejin Choi, et al. Rewardbench: Evaluating reward models for language modeling. *arXiv preprint arXiv:2403.13787*, 2024.
- Guillaume Lample and Devendra Singh Chaplot. Playing FPS Games with Deep Reinforcement Learning. In *Proceedings of the AAAI Conference on Artificial Intelligence*, volume 31, 2017.
- Guiliang Liu and Oliver Schulte. Deep reinforcement learning in ice hockey for context-aware player evaluation. *arXiv preprint arXiv:1805.11088*, 2018.

- Yudong Luo, Oliver Schulte, and Pascal Poupart. Inverse Reinforcement Learning for Team Sports: Valuing Actions and Players. In *Proceedings of the Twenty-Ninth International Joint Conference on Artificial Intelligence (IJCAI-20)*, 2020.
- Saaduddin Mahmud, Saisubramanian Sandhya, and Zilberstein Shlomo. Explanation-Guided Reward Alignment. In *Proceedings of the Thirty-Second International Joint Conference on Artificial Intelligence*, pp. 473–482, 2023.
- Maja J Mataric. Reward Functions for Accelerated Learning. *Machine Learning Proceedings 1994*, pp. pp. 181 – 189, 1994. doi: <https://doi.org/10.1016/B978-1-55860-335-6.50030-1>. URL <https://www.sciencedirect.com/science/article/abs/pii/B9781558603356500301>.
- Eric J Michaud, Adam Gleave, and Stuart Russell. Understanding learned reward functions. *arXiv preprint arXiv:2012.05862*, 2020.
- Andrew Y Ng and Stuart Russell. Algorithms for Inverse Reinforcement Learning. In *International Conference on Machine Learning (ICML)*, volume 2, 2000.
- Andrew Y. Ng, Daishi Harada, and Stuart Russell. Policy Invariance under Reward Transformations: Theory and Application to Reward Shaping. In *International Conference on Machine Learning*, pp. 278–287, 1999.
- Jette Randløv and Preben Alstrøm. Learning to Drive a Bicycle Using Reinforcement Learning and Shaping. In *International Conference on Machine Learning*, volume 98, 1998.
- Jacob Russell and Eugene Santos. Explaining Reward Functions in Markov Decision Processes. In *The Thirty-Second International Flairs Conference*, 2019.
- Eugene Santos and Clement Nyanhongo. A Contextual-Based Framework for Opinion Formation. In *The Thirty-Second International Flairs Conference*, 2019.
- Eugene Santos, Clement Nyanhongo, Hien Nguyen, Keum Joo Kim, and Gregory Hyde. Contextual Evaluation of Human–Machine Team Effectiveness. *Systems Engineering and Artificial Intelligence*, pp. 283–307, 2021.
- David Silver, Satinder Singh, Doina Precup, and Richard S. Sutton. Reward is Enough. *Artificial Intelligence*, 299, 2021.
- Satinder Singh, Richard Lewis, and Andrew G Barto. Where Do Rewards Come From. In *Proceedings of the Annual Conference of the Cognitive Science Society*, pp. pp. 2601 – 2606. Cognitive Science Society, 2009.
- Joar Max Viktor Skalse, Lucy Farnik, Sumeet Ramesh Motwani, Erik Jenner, Adam Gleave, and Alessandro Abate. Starc: A general framework for quantifying differences between reward functions. In *The Twelfth International Conference on Learning Representations*, 2023.
- Halit Bener Suay, Tim Brys, Matthew E. Taylor, and Sonia Chernova. Learning from Demonstration for Shaping through Inverse Reinforcement Learning. In *Proceedings of the 2016 International Conference on Autonomous Agents Multiagent Systems*, pp. 429–437, 2016.
- Richard S Sutton and Andrew G Barto. *Reinforcement Learning: An Introduction*. MIT Press, 2018.
- Ana Tenorio-Gonzalez, Eduardo F. Morales, and Luis Villasenor-Pineda. Dynamic Reward Shaping: Training a Robot by Voice. In *Advances in Artificial Intelligence–IBERAMIA 2010*, pp. 483–492, 2010.
- Garrett Thomas, Yuping Luo, and Tengyu Ma. Safe reinforcement learning by imagining the near future. *Advances in Neural Information Processing Systems*, 34:13859–13869, 2021.
- Stephen Van Evera. Offense, defense, and the causes of war. *International Security*, 22(4):5–43, 1998.
- Oriol Vinyals, Igor Babuschkin, Wojciech M. Czarnecki, Michaël Mathieu, Andrew Dudzik, Junyoung Chung, David H. Choi, T. Ewalds R. Powell, and J. Oh P. Georgiev. Grandmaster Level in StarCraft II using Multi-agent Reinforcement Learning. *Nature*, 575:350–354, 2019.

- Eric Wiewiora, Garrison Cottrell, and Charles Elkan. Principled Methods for Advising Reinforcement Learning Agents. In *Proceedings of the 20th International Conference on Machine Learning*, pp. 792–799, 2003.
- Blake Wulfe, Logan Michael Ellis, Jean Mercat, Rowan Thomas McAllister, and Adrien Gaidon. Dynamics-Aware Comparison of Learned Reward Functions. In *International Conference on Learning Representations (ICLR)*, 2022.
- Markus Wulfmeier, Peter Ondruska, and Ingmar Posner. Maximum Entropy Deep Inverse Reinforcement Learning. preprint arXiv:1507.04888, 2015.
- Chen Yanai, Adir Solomon, Gilad Katz, Bracha Shapira, and Lior Rokach. Q-ball: Modeling basketball games using deep reinforcement learning. In *Proceedings of the AAAI Conference on Artificial Intelligence*, volume 36, pp. 8806–8813, 2022.
- Tom Zahavy, Brendan O’Donoghue, Guillaume Desjardins, and Satinder Singh. Reward is Enough for Convex MDPs. In *Advances in Neural Information Processing Systems*, volume 34, 2021.
- Brian D. Ziebart, Andrew Maas, J.Andrew Bagnell, and Anind K. Dey. Maximum Entropy Inverse Reinforcement Learning. In *Association for the Advancement of Artificial Intelligence (AAAI)*, volume 8, pp. 1433–1438, 2008.

A Derivations, Theorems and Proofs

A.1 Upper Bound Residual Potential for C_{SARD}

The Sparsity Agnostic Canonical Reward is given by:

$$C_{SARD}(R)(s, a, s') = R(s, a, s') + \mathbb{E}[\gamma R(s', A, S_1) - R(s, A, S_2) - \gamma R(S_3, A, S_4) + \gamma^2 R(S_1, A, S_5) - \gamma R(S_2, A, S_6) + \gamma R(S_3, A, S_6) - \gamma^2 R(S_4, A, S_5)],$$

where: S_1 and S_2 are subsequent states to s' and s , respectively; S_3 encompasses all initial states from all transitions; S_4 , S_5 , and S_6 are subsequent states to S_3 , S_1 and S_2 , respectively. For any reward sample, we are guaranteed to compute reliable reward expectations for the first six terms of C_{SARD} , since each set of transitions (S_i, A, S_j) , S_j are created based on S_i , hence they naturally align with any transition distribution. However, for the last two terms, (S_3, A, S_6) and (S_4, A, S_5) , S_5 and S_6 , are not derived from S_4 and S_3 , as they have previously been defined for S_1 and S_2 . Therefore, these two terms can potentially suffer from undersampling, since they require transitions that might not exist in the reward sample distribution. However, C_{SARD} reduces undersampling due to these characteristics:

- Transitions $(S_1, A, S_5) \subseteq (S_4, A, S_5)$, since S_1 are states reached from s' , and S_4 are subsequent states for all transitions, implying that, $(S_1 \subseteq S_4)$.
- With the exception of terminal states in S_2 , transitions $(S_2, A, S_6) \subseteq (S_3, A, S_6)$, since every state in S_2 becomes an initial state for a new transition, ensuring that: $(S_2 \subseteq S_3)$.

Theorem 1: Assuming that transitions $(S_1$ to $S_5)$ and $(S_2$ to $S_6)$ are non-empty, the upper bound residual potential for C_{SARD} is lower than that of C_1 —a modified version of EPIC without assumptions on full transition coverage.

Proof. Consider a reward sample with some unsampled transitions such that the fraction of sampled transitions for (S_4, A, S_5) and (S_3, A, S_6) is p and q , where $0 \leq p, q \leq 1$. Integrating p, q into C_{SARD} :

$$C_{SARD}(R)(s, a, s') = R(s, a, s') + \mathbb{E}[\gamma R(s', A, S_1) - R(s, A, S_2) - \gamma R(S_3, A, S_4) + \gamma^2 R(S_1, A, S_5) - \gamma R(S_2, A, S_6) + q\gamma R(S_3, A, S_6) - p\gamma^2 R(S_4, A, S_5)]$$

Applying C_{SARD} with proportions p, q to a shaped reward $R'(s, a, s')$, we get the residual potential:

$$\phi_{sard} = \mathbb{E}[(\gamma - q\gamma)\phi(S_3) + (p\gamma^2 - \gamma^2)\phi(S_4) + (\gamma^3 - p\gamma^3)\phi(S_5) + (q\gamma^2 - \gamma^2)\phi(S_6)]$$

For C_1 , the residual potential is:

$$\phi_{res1} = \mathbb{E}[\gamma\phi(S_3) + (-\gamma^2)\phi(S_4) + \gamma^2\phi(S_1) + (-\gamma)\phi(S_2)]$$

Comparing the upper bound residual potentials: ϕ_{sard} and ϕ_{res1} .

- For ϕ_{res1} and ϕ_{sard} , each $S_i \subseteq \mathcal{D}_S$, $\forall i \in \{1, \dots, 6\}$, where $\mathcal{D}_S \subseteq \mathcal{S}$ is the state coverage distribution of the reward sample.
- Assuming a finite-sized reward sample, implying that \mathcal{D}_S is finite, each $S_i \subseteq \mathcal{D}_S$ is bounded such that $|\phi(S_i)| \leq M$, where M is the maximum magnitude of potentials, $M \in \mathbb{R}^+$.
- Given that $0 \leq \gamma < 1$; $0 \leq p, q \leq 1$; and $|\phi(S_i)| = M$, $\forall i \in \{1, \dots, 6\}$ (**only considering upper bounds**). For each paired terms in ϕ_{sard} and ϕ_{res1} :

$$|(\gamma - q\gamma)\phi(S_3)| \leq |\gamma\phi(S_3)| \implies |(\gamma - q\gamma)M| \leq |\gamma M| \implies \gamma(1 - q) \leq \gamma \quad (14)$$

$$|(p\gamma^2 - \gamma^2)\phi(S_4)| \leq |(-\gamma^2)\phi(S_4)| \implies |(p\gamma^2 - \gamma^2)M| \leq |(-\gamma^2)M| \implies \gamma^2(1 - p) \leq \gamma^2 \quad (15)$$

$$|(\gamma^3 - p\gamma^3)\phi(S_5)| \leq |\gamma^2\phi(S_1)| \implies |(\gamma^3 - p\gamma^3)M| \leq |\gamma^2 M| \implies \gamma^3(1 - p) \leq \gamma^2 \quad (16)$$

$$|(q\gamma^2 - \gamma^2)\phi(S_6)| \leq |(-\gamma)\phi(S_2)| \implies |(q\gamma^2 - \gamma^2)M| \leq |(-\gamma)M| \implies \gamma^2(1 - q) \leq \gamma \quad (17)$$

Inequalities 14-17, are all true for the given range of values for γ, p, q , and M . Therefore, it's clear that the upper bound residual potential ϕ_{sard} is lower than that of ϕ_{res1} since: $|\phi_{sard}| \leq |\phi_{res1}|$ for all four terms. This relationship is even stronger if both p and q are both greater than 0, converting the above inequalities into strict inequalities. As both p and q approaches 1, the residual shaping is entirely eliminated, making C_{SARD} invariant to shaping. This proof verifies Theorem 1. \square

A.2 The Sparsity Agnostic Canonically Shaped Reward is Invariant to Shaping

Proposition 2: *Let $R : \mathcal{S} \times \mathcal{A} \times \mathcal{S}$ be a reward function, $\phi : \mathcal{S} \rightarrow R$, a state potential function. Given a shaped reward $R'(s, a, s') = R(s, a, s') + \gamma\phi(s') - \phi(s)$, then:*

$$C_{SARD}(R) = C_{SARD}(R').$$

Proof. Lets apply C_{SARD} , Definition 3, to a shaped reward $R'(s, a, s')$:

$$\begin{aligned} C_{SARD}(R')(s, a, s') &= R(s, a, s') + \gamma\phi(s') - \phi(s) + \mathbb{E}[\gamma[R(s', A, S_1) + \gamma\phi(S_1) - \phi(s')]] \\ &\quad - [R(s, A, S_2) + \gamma\phi(S_2) - \phi(s)] - \gamma[R(S_3, A, S_4) + \gamma\phi(S_4) - \phi(S_3)] \\ &\quad + \gamma^2[R(S_1, A, S_5) + \gamma\phi(S_5) - \phi(S_1)] - \gamma[R(S_2, A, S_6) + \gamma\phi(S_6) - \phi(S_2)] \\ &\quad + \gamma[R(S_3, A, S_6) + \gamma\phi(S_6) - \phi(S_3)] - \gamma^2[R(S_4, A, S_5) + \gamma\phi(S_5) - \phi(S_4)], \end{aligned}$$

Regrouping the reward terms and the potentials, this reduces to:

$$\begin{aligned} C_{SARD}(R')(s, a, s') &= C_{SARD}(R)(s, a, s') + (\gamma\phi(s') - \gamma\mathbb{E}[\phi(s')]) + (-\phi(s) + \mathbb{E}[\phi(s)]) \\ &\quad + \mathbb{E}[\gamma^2(\phi(S_1) - \phi(S_1))] + \mathbb{E}[\gamma(-\phi(S_2) + \phi(S_2))] + \mathbb{E}[\gamma(\phi(S_3) - \phi(S_3))] \\ &\quad + \mathbb{E}[-\gamma^2(\phi(S_4) + \phi(S_4))] + \mathbb{E}[\gamma^3(\phi(S_5) - \phi(S_5))] + \mathbb{E}[\gamma^2(-\phi(S_6) + \phi(S_6))] \end{aligned}$$

Since $\mathbb{E}[\gamma\phi(s')] = \gamma\phi(s')$ and $\mathbb{E}[\phi(s)] = \phi(s)$. This leads to:

$$C_{SARD}(R')(s, a, s') = C_{SARD}(R)(s, a, s')$$

\square

A.3 Sample-Based Approximation for SARD

Consider a batch B_V with a coverage distribution B_M , that consists of N_M samples from a joint distribution over states \mathcal{D}_S and actions \mathcal{D}_A . From B_M , we can derive distributions $X_i \subseteq B_M$, for $i \in \{1, \dots, 6\}$. Each X_i is a set, $\{(u, x)\}$, where x is a state and u is an action. The magnitude, $|X_i|$, is denoted by N_i . We define $X_1 = \{(u, x_1)\}$, where x_1 denotes subsequent states for transitions starting from s' ; $X_2 = \{(u, x_2)\}$, where x_2 denotes subsequent states for transitions that start from s . Similarly, $X_3 \dots X_6$ are defined such that $\{(x_3, u, x_4)\}$ encompasses all transitions in the reward sample, where x_3 includes all initial states for all transitions, and x_4 includes all subsequent states for all transitions; $\{(x_1, u, x_5)\}$ are the transitions that start from x_1 with x_5 as the destination; $\{(x_2, u, x_6)\}$ are the transitions that start from x_2 with x_6 as the destination; $\{(x_3, u, x_6)\}$ are the transitions that start from x_3 with x_6 as the destination; and $\{(x_4, u, x_5)\}$ are transitions that start from x_4 with x_5 as the destination. With that, C_{SARD} can be approximated as:

$$\begin{aligned} C_{SARD}(R)(s, a, s') &\approx R(s, a, s') + \frac{\gamma}{N_1} \sum_{(u, x_1) \in B_M} R(s', u, x_1) - \frac{1}{N_2} \sum_{(u, x_2) \in B_M} R(s, u, x_2) \\ &\quad - \frac{\gamma}{N_3 N_4} \sum_{(\cdot, x_3) \in B_M} \sum_{(u, x_4) \in B_M} R(x_3, u, x_4) + \frac{\gamma^2}{N_1 N_5} \sum_{(\cdot, x_1) \in B_M} \sum_{(u, x_5) \in B_M} R(x_1, u, x_5) \\ &\quad - \frac{\gamma}{N_2 N_6} \sum_{(\cdot, x_2) \in B_M} \sum_{(u, x_6) \in B_M} R(x_2, u, x_6) + \frac{\gamma}{N_3 N_6} \sum_{(\cdot, x_3) \in B_M} \sum_{(u, x_6) \in B_M} R(x_3, u, x_6) \\ &\quad - \frac{\gamma^2}{N_4 N_5} \sum_{(\cdot, x_4) \in B_M} \sum_{(u, x_5) \in B_M} R(x_4, u, x_5). \end{aligned} \tag{18}$$

Next, we show that **Proposition 2** holds for the approximation in Equation 18. Applying the sampled-based approximation for $C_{SARD}(R')$ to a potentially shaped reward function R' , we get:

$$\begin{aligned}
C_{SARD}(R')(s, a, s') &\approx R(s, a, s') + \gamma\phi(s') - \phi(s) + \frac{\gamma}{N_1} \sum_{(u, x_1) \in B_M} [R(s', u, x_1) + \gamma\phi(x_1) - \phi(s')] \\
&\quad - \frac{1}{N_2} \sum_{(u, x_2) \in B_M} [R(s, u, x_2) + \gamma\phi(x_2) - \phi(s)] \\
&\quad - \frac{\gamma}{N_3 N_4} \sum_{(\cdot, x_3) \in B_M} \sum_{(u, x_4) \in B_M} [R(x_3, u, x_4) + \gamma\phi(x_4) - \phi(x_3)] \\
&\quad + \frac{\gamma^2}{N_1 N_5} \sum_{(\cdot, x_1) \in B_M} \sum_{(u, x_5) \in B_M} [R(x_1, u, x_5) + \gamma\phi(x_5) - \phi(x_1)] \\
&\quad - \frac{\gamma}{N_2 N_6} \sum_{(\cdot, x_2) \in B_M} \sum_{(u, x_6) \in B_M} [R(x_2, u, x_6) + \gamma\phi(x_6) - \phi(x_2)] \\
&\quad + \frac{\gamma}{N_3 N_6} \sum_{(\cdot, x_3) \in B_M} \sum_{(u, x_6) \in B_M} [R(x_3, u, x_6) + \gamma\phi(x_6) - \phi(x_3)] \\
&\quad - \frac{\gamma^2}{N_4 N_5} \sum_{(\cdot, x_4) \in B_M} \sum_{(u, x_5) \in B_M} [R(x_4, u, x_5) + \gamma\phi(x_5) - \phi(x_4)].
\end{aligned}$$

Rearranging the terms, the above equation can be written as:

$$C_{SARD}(R')(s, a, s') = C_{SARD}(R)(s, a, s') + \phi_{residuals}, \quad (19)$$

where:

$$\begin{aligned}
\phi_{residuals} &= \gamma\phi(s') - \phi(s) + \frac{\gamma}{N_1} \sum_{(u, x_1) \in B_M} [\gamma\phi(x_1) - \phi(s')] - \frac{1}{N_2} \sum_{(u, x_2) \in B_M} [\gamma\phi(x_2) - \phi(s)] \\
&\quad - \frac{\gamma}{N_3 N_4} \sum_{(\cdot, x_3) \in B_M} \sum_{(u, x_4) \in B_M} [\gamma\phi(x_4) - \phi(x_3)] + \frac{\gamma^2}{N_1 N_5} \sum_{(\cdot, x_1) \in B_M} \sum_{(u, x_5) \in B_M} [\gamma\phi(x_5) - \phi(x_1)] \\
&\quad - \frac{\gamma}{N_2 N_6} \sum_{(\cdot, x_2) \in B_M} \sum_{(u, x_6) \in B_M} [\gamma\phi(x_6) - \phi(x_2)] + \frac{\gamma}{N_3 N_6} \sum_{(\cdot, x_3) \in B_M} \sum_{(u, x_6) \in B_M} [\gamma\phi(x_6) - \phi(x_3)] \\
&\quad - \frac{\gamma^2}{N_4 N_5} \sum_{(\cdot, x_4) \in B_M} \sum_{(u, x_5) \in B_M} [\gamma\phi(x_5) - \phi(x_4)].
\end{aligned} \quad (20)$$

For double summations, it can be shown that:

$$\frac{1}{n_1 n_2} \sum_{i=1}^{n_1} \sum_{j=1}^{n_2} (\gamma\phi(x_i) - \phi(x_j)) = \frac{\gamma}{n_1} \sum_{i=1}^{n_1} \phi(x_i) - \frac{1}{n_2} \sum_{j=1}^{n_2} \phi(x_j).$$

Applying this to Equation 20, and simplifying terms, we get:

$$\begin{aligned}
\phi_{residuals} &= \gamma\phi(s') - \phi(s) + \frac{\gamma^2}{N_1} \sum_{(u, x_1) \in B_M} [\phi(x_1)] - \gamma\phi(s') - \frac{\gamma}{N_2} \sum_{(u, x_2) \in B_M} [\phi(x_2)] + \phi(s) \\
&\quad - \frac{\gamma^2}{N_4} \sum_{(\cdot, x_4) \in B_M} [\phi(x_4)] + \frac{\gamma}{N_3} \sum_{(\cdot, x_3) \in B_M} [\phi(x_3)] + \frac{\gamma^3}{N_5} \sum_{(\cdot, x_5) \in B_M} [\phi(x_5)] - \frac{\gamma^2}{N_1} \sum_{(\cdot, x_1) \in B_M} [\phi(x_1)] \\
&\quad - \frac{\gamma^2}{N_6} \sum_{(\cdot, x_6) \in B_M} [\phi(x_6)] + \frac{\gamma}{N_2} \sum_{(\cdot, x_2) \in B_M} [\phi(x_2)] + \frac{\gamma^2}{N_6} \sum_{(\cdot, x_6) \in B_M} [\phi(x_6)] - \frac{\gamma}{N_3} \sum_{(\cdot, x_3) \in B_M} [\phi(x_3)] \\
&\quad - \frac{\gamma^3}{N_5} \sum_{(\cdot, x_5) \in B_M} [\phi(x_5)] + \frac{\gamma^2}{N_4} \sum_{(\cdot, x_4) \in B_M} [\phi(x_4)] = 0
\end{aligned}$$

Therefore, **Proposition 2**, $C_{SARD}(R')(s, a, s') = C_{SARD}(R)(s, a, s')$ is satisfied using the SARD approximation. However, a much faster approximation can be achieved as follows:

$$\begin{aligned}
C_{SARD}(R)(s, a, s') \approx & R(s, a, s') + \frac{\gamma}{T_{(s', x_1)}} \sum_{(u, x_1) \in B_M} R(s', u, x_1) \\
& - \frac{1}{T_{(s, x_2)}} \sum_{(u, x_2) \in B_M} R(s, u, x_2) - \frac{\gamma}{T_{(x_3, x_4)}} \sum_{(u, x_4) \in B_M} R(x_3, u, x_4) \\
& + \frac{\gamma^2}{T_{(x_1, x_5)}} \sum_{(u, x_5) \in B_M} R(x_1, u, x_5) - \frac{\gamma}{T_{(x_2, x_6)}} \sum_{(u, x_6) \in B_M} R(x_2, u, x_6) \\
& + \frac{\gamma}{T_{(x_3, x_6)}} \sum_{(u, x_6) \in B_M} R(x_3, u, x_6) - \frac{\gamma^2}{T_{(x_4, x_5)}} \sum_{(u, x_5) \in B_M} R(x_4, u, x_5),
\end{aligned} \tag{21}$$

where $T_{(i,j)}$ denotes the number of transitions from states in i to states in j .

A.4 Generalized SARD Extensions

The following steps result in the generalized formula for potential SARD extensions.

1. To eliminate EPIC's need for full coverage (Section 4), we first create C_1 to ensure that rewards are canonicalized based on actual transition sample distributions:

$$C_1(R)(s, a, s') = R(s, a, s') + \mathbb{E}[\gamma R(s', A, S_1) - R(s, A, S_2) - \gamma R(S_3, A, S_4)].$$

C_1 yields a residual potential: $\phi_{res1} = \mathbb{E}[\gamma^2 \phi(S_1) - \gamma^2 \phi(S_4) + \gamma \phi(S_3) - \gamma \phi(S_2)]$.

2. To cancel $\mathbb{E}[\phi(S_i)]$, $\forall i \in \{1, \dots, 4\}$, we add rewards $R(S_i, A, k_i^1)$ to induce potentials $\gamma \phi(k_i^1) - \phi(S_i)$, which results in C_2 :

$$\begin{aligned}
C_2(R)(s, a, s') = & R(s, a, s') + \mathbb{E}[\gamma R(s', A, S_1) - R(s, A, S_2) - \gamma R(S_3, A, S_4) \\
& + \gamma^2 R(S_1, A, k_1^1) - \gamma^2 R(S_4, A, k_4^1) + \gamma R(S_3, A, k_3^1) - \gamma R(S_2, A, k_2^1)].
\end{aligned}$$

C_2 yields a residual potential: $\phi_{res2} = \mathbb{E}[\gamma^3 \phi(k_1^1) - \gamma^3 \phi(k_4^1) + \gamma^2 \phi(k_3^1) - \gamma^2 \phi(k_2^1)]$.

3. To cancel $\mathbb{E}[\phi(k_i^1)]$, we add rewards $R(k_i^1, A, k_i^2)$ to induce potentials $\gamma \phi(k_i^2) - \phi(k_i^1)$, yielding C_3 :

$$\begin{aligned}
C_3(R)(s, a, s') = & R(s, a, s') + \mathbb{E}[\gamma R(s', A, S_1) - R(s, A, S_2) - \gamma R(S_3, A, S_4) \\
& + \gamma^2 R(S_1, A, k_1^1) - \gamma^2 R(S_4, A, k_4^1) + \gamma R(S_3, A, k_3^1) - \gamma R(S_2, A, k_2^1) \\
& + \gamma^3 R(k_1^1, A, k_1^2) - \gamma^3 R(k_4^1, A, k_4^2) + \gamma^2 R(k_3^1, A, k_3^2) - \gamma^2 R(k_2^1, A, k_2^2)]
\end{aligned}$$

C_3 yields a residual potential: $\phi_{res3} = \mathbb{E}[\gamma^4 \phi(k_1^2) - \gamma^4 \phi(k_4^2) + \gamma^3 \phi(k_3^2) - \gamma^3 \phi(k_2^2)]$.

4. As we can see, this process results in the generalized formula:

$$\begin{aligned}
C_n(R)(s, a, s') = & R(s, a, s') + \mathbb{E}[\gamma R(s', A, S_1) - R(s, A, S_2) - \gamma R(S_3, A, S_4) \\
& + \gamma^2 R(S_1, A, k_1^1) - \gamma^2 R(S_4, A, k_4^1) + \gamma R(S_3, A, k_3^1) - \gamma R(S_2, A, k_2^1) \\
& + \gamma^3 R(k_1^1, A, k_1^2) - \gamma^3 R(k_4^1, A, k_4^2) + \gamma^2 R(k_3^1, A, k_3^2) - \gamma^2 R(k_2^1, A, k_2^2) \\
& \dots \\
& + \gamma^n R(k_1^{n-2}, A, k_1^{n-1}) - \gamma^n R(k_4^{n-2}, A, k_4^{n-1}) + \gamma^{n-1} R(k_3^{n-2}, A, k_3^{n-1}) - \gamma^{n-1} R(k_2^{n-2}, A, k_2^{n-1})],
\end{aligned}$$

where, $n \geq 3$. C_n yields a residual potential:

$$\phi_n = \mathbb{E}[\gamma^{n+1} \phi(k_1^{n-1}) - \gamma^{n+1} \phi(k_4^{n-1}) + \gamma^n \phi(k_3^{n-1}) - \gamma^n \phi(k_2^{n-1})].$$

- Looking at ϕ_n , as n increases, we generally multiply the state distributions, k_i by $(\approx \gamma^n)$. Therefore, the upper bound magnitude of ϕ_n significantly decreases since $0 \leq \gamma < 1$, and each $|\phi(k_i)| \leq M$, where M is the upper bound potential for all distributions $k_i \subseteq \mathcal{D}_S$ (see Appendix A.1). Therefore, as n approaches infinity, ϕ_n approaches 0.
- The advantage of the generalized SARD form is that ϕ_n approaches 0 as n increases, without any assumptions on the distribution of a reward sample. The challenge, however, is that many k_i terms need to be computed making the process very expensive and difficult to implement. Therefore, a smaller n is preferable. In SARD, we choose $n = 2$, then use our intuition to select sets, k_i , which further reduces the residual potential.

A.5 Residual Potentials

Residual potentials can be defined as the remaining sum of potentials after reward canonicalization.

Derivation of ϕ_{res1} : As shown in Section 4, the equation for $C_1(R)(s, a, s')$ is:

$$C_1(R)(s, a, s') = R(s, a, s') + \mathbb{E}[\gamma R(s', A, S_1) - R(s, A, S_2) - \gamma R(S_3, A, S_4)],$$

Applying C_1 to a shaped reward $R'(s, a, s') = R(s, a, s') + \gamma\phi(s') - \phi(s)$:

$$\begin{aligned} C_1(R')(s, a, s') &= R'(s, a, s') + \mathbb{E}[\gamma R'(s', A, S_1) - R'(s, A, S_2) - \gamma R'(S_3, A, S_4)] \\ &= R(s, a, s') + \gamma\phi(s') - \phi(s) + \mathbb{E}[\gamma(R(s', A, S_1) + \gamma\phi(S_1) - \phi(s')) \\ &\quad - (R(s, A, S_2) + \gamma\phi(S_2) - \phi(s)) - \gamma(R(S_3, A, S_4) + \gamma\phi(S_4) - \phi(S_3))] \\ &= C_1(R)(s, a, s') + \mathbb{E}[\gamma^2\phi(S_1) - \gamma^2\phi(S_4) + \gamma\phi(S_3) - \gamma\phi(S_2)] \end{aligned}$$

Hence, $C_1(R)(s, a, s')$ yields the residual potential:

$$\phi_{res1} = \mathbb{E}[\gamma^2\phi(S_1) - \gamma^2\phi(S_4) + \gamma\phi(S_3) - \gamma\phi(S_2)].$$

Derivation of ϕ_{res2} : As shown in Section 4, the equation for $C_2(R)(s, a, s')$ is:

$$\begin{aligned} C_2(R)(s, a, s') &= R(s, a, s') + \mathbb{E}[\gamma R(s', A, S_1) - R(s, A, S_2) - \gamma R(S_3, A, S_4) + \gamma^2 R(S_1, A, k_1) \\ &\quad - \gamma R(S_2, A, k_2) + \gamma R(S_3, A, k_3) - \gamma^2 R(S_4, A, k_4)]. \end{aligned}$$

Applying C_2 to shaped reward $R'(s, a, s') = R(s, a, s') + \gamma\phi(s') - \phi(s)$:

$$\begin{aligned} C_2(R')(s, a, s') &= R(s, a, s') + \gamma\phi(s') - \phi(s) + \mathbb{E}[\gamma(R(s', A, S_1) + \gamma\phi(S_1) - \phi(s')) \\ &\quad - (R(s, A, S_2) + \gamma\phi(S_2) - \phi(s)) - \gamma(R(S_3, A, S_4) + \gamma\phi(S_4) - \phi(S_3)) \\ &\quad + \gamma^2(R(S_1, A, k_1) + \gamma\phi(k_1) - \phi(S_1)) - \gamma(R(S_2, A, k_2) + \gamma\phi(k_2) - \phi(S_2)) \\ &\quad + \gamma(R(S_3, A, k_3) + \gamma\phi(k_3) - \phi(S_3)) - \gamma^2(R(S_4, A, k_4) + \gamma\phi(k_4) - \phi(S_4))] \\ &= C_2(R)(s, a, s') + \mathbb{E}[\gamma^3\phi(k_1) - \gamma^3\phi(k_4) + \gamma^2\phi(k_3) - \gamma^2\phi(k_2)] \end{aligned}$$

Hence, $C_2(R)(s, a, s')$ yields the residual potential:

$$\phi_{res2} = \mathbb{E}[\gamma^3\phi(k_1) - \gamma^3\phi(k_4) + \gamma^2\phi(k_3) - \gamma^2\phi(k_2)].$$

A.6 Pseudometric Equivalence Under Full Coverage

Proposition 3. *The SARD, DARD, and EPIC canonical rewards are similar when a reward function has full coverage.*

Proof.

$$C_{EPIC}(R)(s, a, s') = R(s, a, s') + \mathbb{E}[\gamma R(s', A, S') - R(s, A, S') - \gamma R(S, A, S')]$$

$$C_{DARD}(R)(s, a, s') = R(s, a, s') + \mathbb{E}[\gamma R(s', A, S') - R(s, A, S') - \gamma R(S', A, S')]$$

$$\begin{aligned} C_{SARD}(R)(s, a, s') &= R(s, a, s') + \mathbb{E}[\gamma R(s', A, S_1) - R(s, A, S_2) - \gamma R(S_3, A, S_4) \\ &\quad + \gamma^2 R(S_1, A, S_5) - \gamma R(S_2, A, S_6) + \gamma R(S_3, A, S_6) - \gamma^2 R(S_4, A, S_5)] \end{aligned}$$

If a reward function has full coverage, every state $s \in S$, is connected by A actions to every other state $s' \in S$. Thus, $S = S' = S'' = S_1 = S_2 = S_3 = S_4 = S_5 = S_6$, such that:

$$C_{EPIC} = C_{DARD} = C_{SARD} = R(s, a, s') + \mathbb{E}[\gamma R(s', A, S) - R(s, A, S) - \gamma R(S, A, S)].$$

□

A.7 Repeated Canonicalization Under Full Coverage

Proposition 4. *The SARD, DARD, or EPIC canonical reward cannot be further canonicalized if the reward function has full coverage.*

From Proposition 3, under full coverage:

$$C_S = C_{EPIC} = C_{DARD} = C_{SARD} = R(s, a, s') + \mathbb{E}[\gamma R(s', A, S) - R(s, A, S) - \gamma R(S, A, S)].$$

Applying Equation 16, to canonicalize a previously canonical reward we get:

$$\begin{aligned} C_S[C_S(R)(s, a, s')] &= C_S[R(s, a, s') + \mathbb{E}[\gamma R(s', A, S) - R(s, A, S) - \gamma R(S, A, S)]] \\ &= C_S(R(s, a, s')) + \gamma \mathbb{E}[C_S(R(s', A, S))] - \mathbb{E}[C_S(R(s, A, S))] - \gamma \mathbb{E}[C_S(R(S, A, S))] \\ &= C_S(R)(s, a, s') + \gamma \mathbb{E}[C_S[R(s', a, S) + \mathbb{E}[\gamma R(S, A, S) - R(s', A, S) - \gamma R(S, A, S)]]] \\ &\quad - \mathbb{E}[C_S[R(s, a, S) + \mathbb{E}[\gamma R(S, A, S) - R(s, A, S) - \gamma R(S, A, S)]]] \\ &\quad - \gamma \mathbb{E}[C_S[R(S, a, S) + \mathbb{E}[\gamma R(S, A, S) - R(S, A, S) - \gamma R(S, A, S)]]] \\ &= C_S(R)(s, a, s') + \gamma \mathbb{E}[C_S[(R(s', A, S) - \mathbb{E}[R(s', A, S)]) + \mathbb{E}[\gamma R(S, A, S) - \gamma R(S, A, S)]]] \\ &\quad - \mathbb{E}[C_S[(R(s, A, S) - \mathbb{E}[R(s, A, S)]) + \mathbb{E}[\gamma R(S, A, S) - \gamma R(S, A, S)]]] \\ &\quad - \gamma \mathbb{E}[C_S[R(S, a, S) + \mathbb{E}[\gamma R(S, A, S) - R(S, A, S) - \gamma R(S, A, S)]]] \end{aligned}$$

After explicit cancellations, the above equation reduces to:

$$C_S[C_S(R)(s, a, s')] = C_S(R)(s, a, s').$$

A.8 Regret Bound

In this section, we establish a regret bound in terms of the SARD distance. The procedure for the analysis is adapted from related work on EPIC by Gleave et al. (2020).

Given reward functions R_A and R_B and their optimal policies π_A^* and π_B^* , we show that the regret of using policy π_B^* instead of a policy π_A^* is bounded by a function of $D_{SARD}(R_A, R_B)$. We also show that as the regret tends to be 0 suggesting that $\pi_A^* \approx \pi_B^*$, the distance, $D_{SARD}(R_A, R_B) \rightarrow 0$. The concept of regret bounds is important as it shows that differences in D_{SARD} reflect differences between optimal policies induced by the input rewards.

For our analysis, we will use the following Lemmas:

Lemma 1. *Let f be a one-dimensional vector of real numbers and $f_i \subseteq f$. Then:*

$$\|f_i\|_2 \leq \|f\|_2 \quad (22)$$

Proof. Suppose f has n elements and f_i has k elements. Since $f_i \subseteq f$, every element in f_i is also in f , and $k \leq n$. Therefore, $f^2 \geq f_i^2$ (Euclidean distance always positive) such that: $\|f_i\|_2 \leq \|f\|_2$. \square

Lemma 2. *Let $R_A, R_B : S \times A \times S \rightarrow \mathbb{R}$ be reward functions with corresponding optimal policies π_A^* and π_B^* . Let $D_\pi(t, s_t, a_t, s_{t+1})$ denote the distribution over trajectories that policy π induces at time step t . Let $D(s, a, s')$ be the coverage distribution over transitions $S \times A \times S$. Suppose that there exists some $K > 0$ such that $KD(s_t, a_t, s_{t+1}) \geq D(t, s_t, a_t, s_{t+1})$ for all time steps $t \in \mathbb{N}$, triples $s_t, a_t, s_{t+1} \in S \times A \times S$ and policies $\pi \in \{\pi_A^*, \pi_B^*\}$. Then the regret under R_A from executing π_B^* optimal for R_B instead of π_A^* is at most:*

$$G_{R_A}(\pi_A^*) - G_{R_A}(\pi_B^*) \leq \frac{2K}{1-\gamma} D_{L_1, D}(R_A, R_B).$$

where: $D_{L_1, D}$ is either a metric or pseudometric in L_1 space, and $G_R(\pi)$ resembles the return of R under a policy π .

Proof. See Gleave et al. (2020) \square

Lemma 3. *Let $R_A, R_B : S \times A \times S \rightarrow \mathbb{R}$ be reward functions. Let π_A^* and π_B^* be policies optimal for rewards R_A and R_B . Suppose the regret under the standardized reward R_A^{SARD} from executing π_B^* instead of π_A^* is upper bounded by some $U \in \mathbb{R}$:*

$$G_{R_A^{SARD}}(\pi_A^*) - G_{R_A^{SARD}}(\pi_B^*) \leq U. \quad (23)$$

Then the regret under the original reward R_A is bounded by:

$$G_{R_A}(\pi_A^*) - G_{R_A}(\pi_B^*) \leq 8U \|R_A\|_2. \quad (24)$$

Proof. Let the standardized reward can be represented as:

$$R^{SARD} = \frac{C_{SARD}(R)}{\|C_{SARD}(R)\|_2}, \quad (25)$$

It follows that:

$$G_{R^{SARD}}(\pi) = \frac{1}{\|C_{SARD}(R)\|_2} G_{C_{SARD}(R)}(\pi) = \frac{1}{\|C_{SARD}(R)\|_2} (G_R(\pi) - \mathbb{E}_{s_0 \sim d_0}[\Phi(s_0)]), \quad (26)$$

where, s_0 depends only on the initial state distribution d_0 , but not π . Applying Equation 26 to π_A^* and π_B^* :

$$G_{R^{SARD}}(\pi_A^*) - G_{R^{SARD}}(\pi_B^*) = \frac{1}{\|C_{SARD}(R_A)\|_2} (G_{R_A}(\pi_A^*) - G_{R_A}(\pi_B^*)). \quad (27)$$

Combining Equation 27 and 23:

$$G_{R_A}(\pi_A^*) - G_{R_A}(\pi_B^*) \leq U \|C_{SARD}(R_A)\|_2. \quad (28)$$

We now bound $\|C_{SARD}(R_A)\|_2$ in terms of $\|R_A\|_2$. The SARD canonical reward is expressed as:

$$\begin{aligned} C_{SARD}(R)(s, a, s') &= R(s, a, s') + \mathbb{E}[\gamma R(s', A, S_1) - R(s, A, S_2) - \gamma R(S_3, A, S_4) \\ &\quad + \gamma^2 R(S_1, A, S_5) - \gamma R(S_2, A, S_6) + \gamma R(S_3, A, S_6) - \gamma^2 R(S_4, A, S_5)] \end{aligned}$$

Now, using the triangular equality rule on the L_2 distance, and linearity of expectation:

$$\begin{aligned} \|C_{SARD}(R)(s, a, s')\|_2 &\leq \|R(s, a, s')\|_2 + \mathbb{E}[\gamma \|R(s', A, S_1)\|_2 + \| - R(s, A, S_2) \|_2 + \gamma \| - R(S_3, A, S_4) \|_2 \\ &\quad + \gamma^2 \|R(S_1, A, S_5)\|_2 + \gamma \| - R(S_2, A, S_6) \|_2 + \gamma \|R(S_3, A, S_6)\|_2 + \gamma^2 \| - R(S_4, A, S_5) \|_2] \end{aligned}$$

Using Lemma 1, the L_2 norm of each reward subspace is such that:

$$\|R(S_i, A_j, S_k)\|_2 \leq \|R(S, A, S')\|_2 = \|R\|_2. \quad (29)$$

therefore,

$$\|C_{SARD}(R)(s, a, s')\|_2 \leq 8\|R\|_2 \quad (30)$$

Combining Equation 30 and 28 we get:

$$G_{R_A}(\pi_A^*) - G_{R_A}(\pi_B^*) \leq 8U\|R\|_2.$$

□

Theorem 2. Let $R_A, R_B : S \times A \times S \rightarrow \mathbb{R}$ be reward functions with respective optimal policies, π_A^*, π_B^* . Let $D_\pi(t, s_t, a_t, s_{t+1})$ be the distribution over transitions $S \times A \times S$ induced by policy π at time t , and $D(s, a, s')$ be the coverage distribution. Suppose there exists $K > 0$ such that $KD(s_t, a_t, s_{t+1}) \geq D_\pi(t, s_t, a_t, s_{t+1})$ for all times $t \in \mathbb{N}$, triples $(s_t, a_t, s_{t+1}) \in S \times A \times S$ and policies $\pi \in \{\pi_A^*, \pi_B^*\}$. Then the regret under R_A from executing π_B^* instead of π_A^* is at most:

$$G_{R_A}(\pi_A^*) - G_{R_A}(\pi_B^*) \leq 32K\|R_A\|_2(1-\gamma)^{-1}D_{SARD}(R_A, R_B),$$

where $G_R(\pi)$ is the return of policy π under reward R .

Proof. Adapting Gleave et al. (2020) [A.4], we can write:

$$D_{SARD}(R_A, R_B) = \frac{1}{2} \|R_A^{SARD}(S, A, S') - R_B^{SARD}(S, A, S')\|_2^2. \quad (31)$$

such that, when considering the L_1 distance:

$$D_{L_1, D}(R_A^{SARD}, R_B^{SARD}) = \|R_A^{SARD}(S, A, S') - R_B^{SARD}(S, A, S')\|_1 \leq 2D_{SARD}(R_A, R_B). \quad (32)$$

Combining Lemma 2 and Equation 32:

$$G_{R_A^{SARD}}(\pi_A^*) - G_{R_A^{SARD}}(\pi_B^*) \leq \frac{2K}{1-\gamma} D_{L_1, D}(R_A^{SARD}, R_B^{SARD}) \leq \frac{4K}{1-\gamma} D_{SARD}(R_A, R_B). \quad (33)$$

Applying Lemma 3, we get:

$$G_{R_A}(\pi_A^*) - G_{R_A}(\pi_B^*) \leq \frac{32K\|R_A\|_2}{1-\gamma} D_{SARD}(R_A, R_B). \quad (34)$$

□

As shown, when $D_{SARD} \rightarrow 0$, the regret goes towards 0.

A.9 Computational Considerations

Given a reward sample composed of N_T transitions that span a state space $S \subseteq \mathcal{S}$ and an action space $A \subseteq \mathcal{A}$. The computational complexity for: $C_{SARD} \approx O(N_T^2)$; $C_{DARD} \approx O(N_T^2)$; and $C_{EPIC} \approx O(N_T)$.

EPIC Complexity:

$$C_{EPIC}(R)(s, a, s') = R(s, a, s') + \mathbb{E}[\gamma R(s', A, S') - R(s, A, S') - \gamma R(S, A, S')].$$

- Given N_T transitions, we can compute $\mathbb{E}[R(S, A, S')]$ in one traversal, and gather transitions (s, A, S') , using a dictionary in constant time within the same traversal ($\approx O(N_T)$).
- In one traversal, we can compute $\sum R(s, A, s')$; $\sum R(s, A, S')$; and $\sum R(s', A, S')$, allowing us to get reward expectations in $O(N_T)$.
- Hence, the overall complexity $\approx O(N_T)$.

DARD Complexity:

$$C_{DARD}(R)(s, a, s') = R(s, a, s') + \mathbb{E}[\gamma R(s', A, S'') - R(s, A, S') - \gamma R(S', A, S'')].$$

- Using a dictionary where each key is a state, each value is a tuple storing the sum, frequency, and dictionary of next states (*sum, frequency, next_states*): we can gather transitions (s, A, S') in one traversal, hence the computational cost for such a computation $\approx O(N_T)$.
- For each (s, a, s') transition, we retrieve S_1 and S_2 (from the dictionary) in constant time, and take a full pass through N_T transitions, to compute $\sum R(S', A, S'')$ at a cost $\approx O(N_T^2)$.
- Hence, the overall complexity $\approx O(N_T^2)$.

SARD Complexity:

$$C_{SARD}(R)(s, a, s') = R(s, a, s') + \mathbb{E}[\gamma R(s', A, S_1) - R(s, A, S_2) - \gamma R(S_3, A, S_4) + \gamma^2 R(S_1, A, S_5) - \gamma R(S_2, A, S_6) + \gamma R(S_3, A, S_6) - \gamma^2 R(S_4, A, S_5)].$$

- Given N_T transitions, we can compute the average reward for the entire sample, $\mathbb{E}[R(S_3, A, S_4)]$; and get the sets (S_3, S_4) in one traversal, $O(N_T)$.
- Using a dictionary where each key is a state, each value is a tuple storing the sum, frequency, and dictionary of next states (*sum, frequency, next_states*): we can compute transitions (s, A, S') in one traversal, $\approx O(N_T)$.
- For each transition s, a, s' :
 - We can retrieve (S_1, S_2) from the dictionary at constant time.
 - Using S_1 and S_2 we can find S_5 and S_6 in one traversal of N_T , as well as compute $\sum R(S_1, A, S_5)$ and $\sum R(S_2, A, S_6)$.
 - Using precomputed S_3 and S_4 , we can estimate $\sum R(S_4, A, S_5)$ and $\sum R(S_3, A, S_6)$ in one traversal.
 - Aggregating everything, we can compute all the expectation terms in $\approx O(N_T^2)$.
- Hence, the overall complexity $\approx O(N_T^2)$.
- SARD has more computations than DARD, however, their asymptotic performances are theoretically of the same order.

B Experiment 1: Additional Analysis

B.1 Reward Functions

Extrinsic reward values are manually defined using a combination of state and action features. For the Starcraft2 and Drone Combat domains, we use the default game score (also based on state and action features), as the reward values. For the Gridworld and Bouncing Balls domains, in each reward function, the reward value, $R(s, a, s')$; is derived from the decomposition of state and action features, where, (s_{f1}, \dots, s_{fn}) is from the starting state, s ; (a_{f1}, \dots, a_{fm}) is from the action, a ; and $(s'_{f1}, \dots, s'_{fn})$ is from the subsequent state, s' . For the Gridworld domain, these features are the (x, y) coordinates, and for the Bouncing Balls domain, these include (x, y, d) , where d is the distance of the obstacle nearest to the ball. Using the following randomly generated constants: $\{u_1, \dots, u_n\}$ for incoming state features; $\{w_1, \dots, w_m\}$ for action features; $\{v_1, \dots, v_n\}$ for subsequent state features; we created the following reward models:

- Linear:

$$R(s, a, s') = u_1 s_{f1} + \dots + u_n s_{fn} + w_1 a_{f1} + \dots + w_m a_{fm} + v_1 s'_{f1} + \dots + v_n s'_{fn},$$

- Polynomial:

$$R(s, a, s') = u_1 s_{f1}^\alpha + \dots + u_n s_{fn}^\alpha + w_1 a_{f1}^\alpha + \dots + w_m a_{fm}^\alpha + v_1 s'_{f1}^\alpha + \dots + v_n s'_{fn}^\alpha,$$

where, α is randomly generated from 1 – 10, denoting the degree of the polynomial.

- Sinusoidal:

$$R(s, a, s') = u_1 \sin(s_{f1}) + \dots + u_n \sin(s_{fn}) + w_1 \sin(a_{f1}) + \dots + w_m \sin(a_{fm}) \\ + v_1 \sin(s'_{f1}) + \dots + v_n \sin(s'_{fn})$$

- Random

$$R(s, a, s') = \beta,$$

where, β is a randomly generated reward for each given transition.

The same relationships are used to model potential functions, where: $\phi(s) = f(s_{f1}, \dots, s_{fn})$, and f is the relationship drawn from the set: {polynomial, sinusoidal, linear, random}. For the Starcraft 2 and Drone Combat domains, we used the default game score provided the game engine, as the reward function. For the Starcraft2 domain, this score⁴ focuses on the composition of unit and resource features as well as actions within the domain. Since the Drone Combat environment is originally designed for a predator-prey domain, we adapt the score⁵ to essentially work the same for the Drone Combat scene (i.e instead of a predator being rewarded for eating some prey, the reward is now an ally attacking an enemy).

⁴<https://steemit.com/steemstem/@cpufroz/building-a-bot-for-starcraft-ii-2-the-starcraft-ii-environment>

⁵https://github.com/koulanurag/ma-gym/blob/master/ma_gym/envs/

B.2 Transition Sparsity Experiment

Algorithm 1 summarizes the pseudocode for Experiment 1 to examine transition sparsity. To test the effect of limited sampling, we run the algorithm with different number of rollouts (rollout count), dictated by the array T . To test the effect of feasibility constraints, we run Algorithm 1 but with imposed movement restrictions by setting $\epsilon = 0$.

Algorithm 1 Analyzing the effect of limited sampling on reward distance

Input:

T - list of policy rollout counts,
 E - number of experimental trials under same condition,
 G - grid size,
 RD - list to store reward distances at different coverages,
 MC - maximum coverage $\approx S \times A \times S$.

Output: RD

```

1: generate  $GT$  - ground truth reward,  $SH$  - shaped reward from all possible transitions.
2: for  $rollout\_count$  in  $T$  do
3:    $trial\_distance, trial\_coverage = \text{list}(), \text{list}()$ 
4:   for  $trial$  in  $E$  do
5:      $B_{gt}, B_{sh} = \text{set}(), \text{set}()$ 
6:     generate trajectories  $\tau_{gt}$  and  $\tau_{sh}$  using uniform policy rollouts.
7:     for  $(s, a, s') \in \tau_{gt}$  do
8:        $B_{gt}.\text{add}(s, a, s')$ 
9:     end for
10:    for  $(s, a, s') \in \tau_{sh}$  do
11:       $B_{sh}.\text{add}(s, a, s')$ 
12:    end for
13:    for  $(s, a, s') \in B_{gt}$ , and  $(s, a, s') \in B_{sh}$  retrieve  $R(s, a, s')$  using  $GT$  and  $R'(s, a, s')$  using  $SH$ , respectively.
14:     $coverage = |B_{gt} \cup B_{sh}| / MC$ 
15:    compute  $dist(R, R')$  using EPIC, SARD, DARD, or other comparison metrics.
16:     $trial\_distance.\text{append}(dist(R, R'))$ 
17:     $trial\_coverage.\text{append}(coverage)$ 
18:  end for
19:   $RD.\text{append}([\text{mean}(trial\_coverage), \text{mean}(trial\_distance)])$ 
20: end for

```

B.3 Experimental Parameters

A uniform policy in the Gridworld domain, would randomly select one of the four actions, {north, east, south, west}, at each timestep. For the Bouncing Balls domain, it would select {north, north-east, east, east-south, south, south-west, west, west-north, north}, randomly. The parameter ϵ dictates the ratio of times in which random transitions (instead of uniform policy), are executed. Table 2 and Table 3 shows the experimental parameters used to run Experiment 1 (Algorithm 1).

Table 2: Low Coverage: Parameters used to test the variation of coverage for the Gridworld and the Bouncing Balls domain.

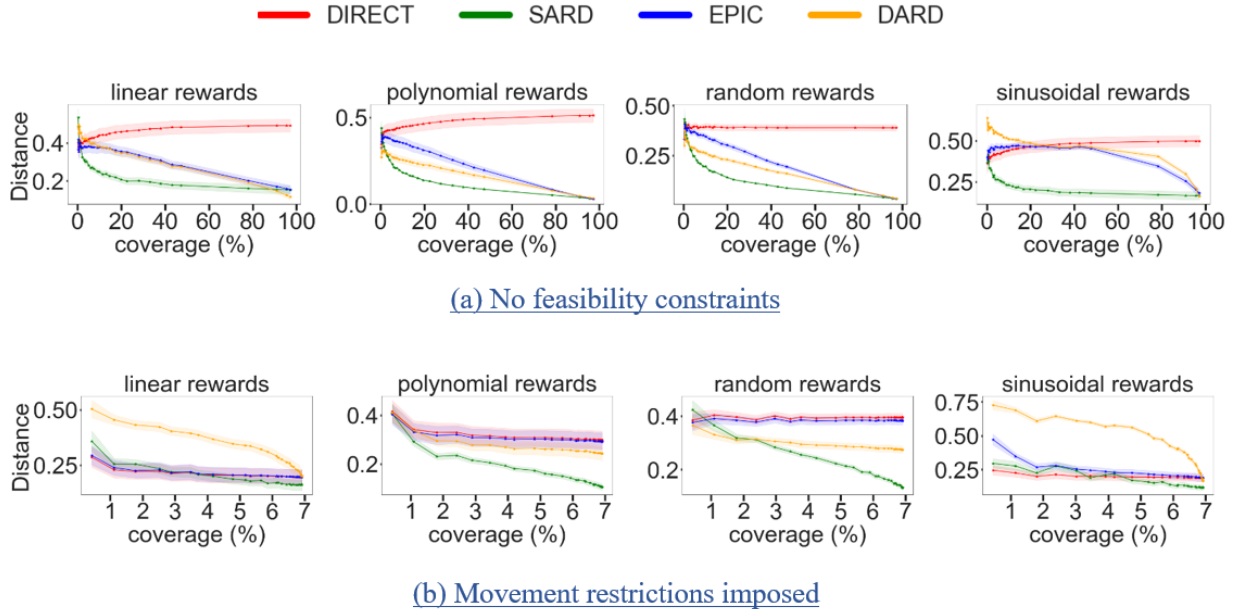
Parameter	Values
Rollout Counts, T	[1, 2, 3, 4, 5, 6, 7, 8, 9, 10, 15, 20, 30, 40, 50, 75, 100, 200, 300, 400, 500, 1000, 2000]
Epochs, E	200
Policy, π	uniform, $\epsilon = 0.1$
Discount, γ	0.7
Dimensions	20×20

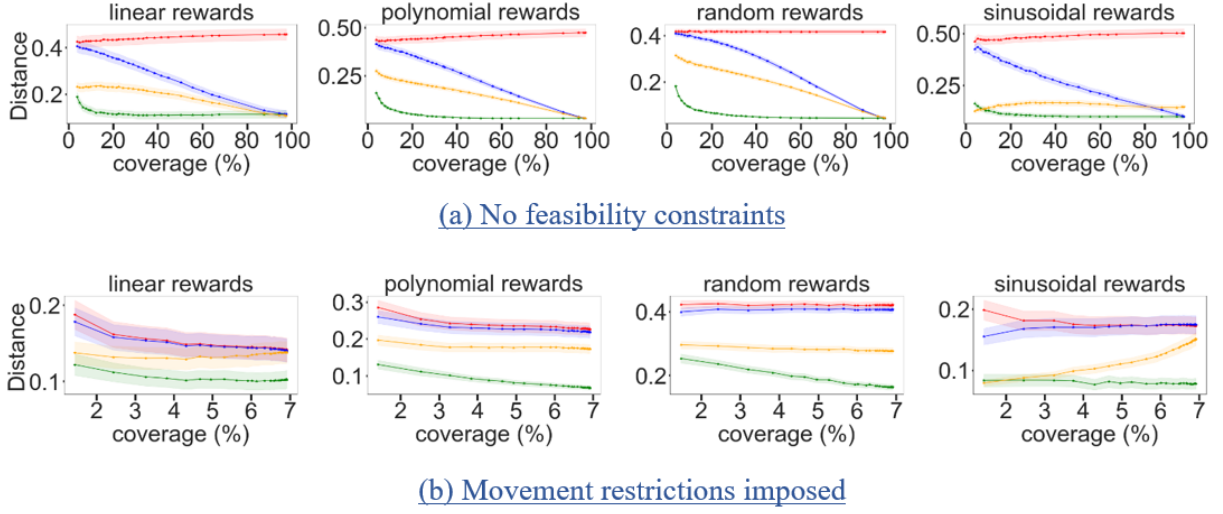
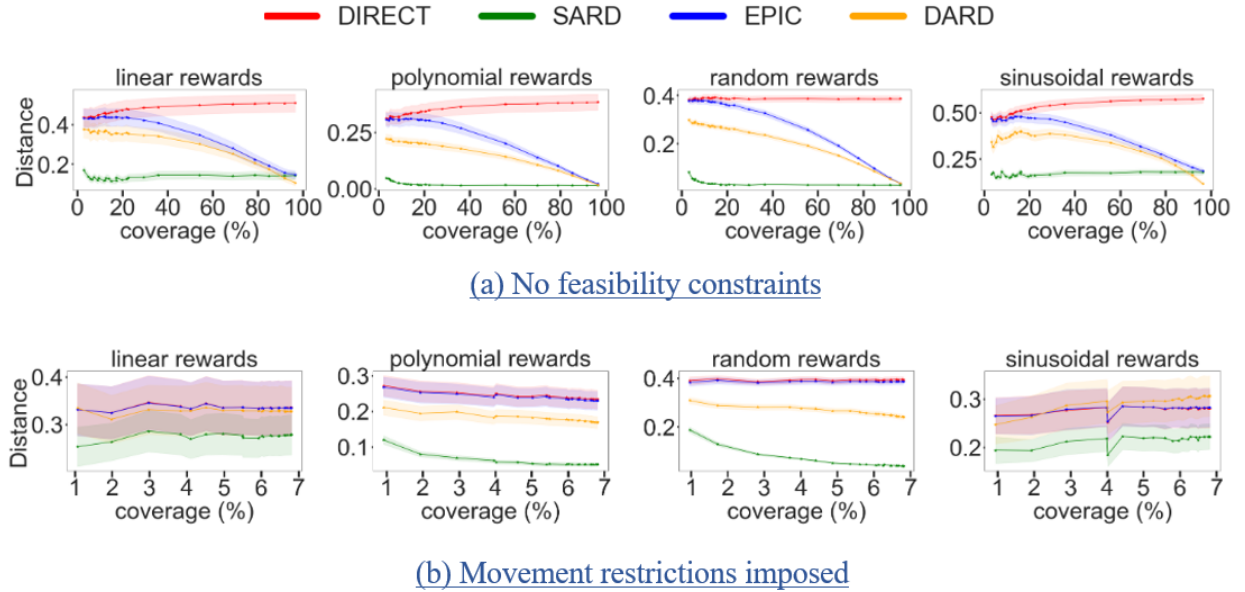
Table 3: Feasibility Constraints: Parameters used to test the variation of coverage in the presence of movement restrictions, $\epsilon = 0$.

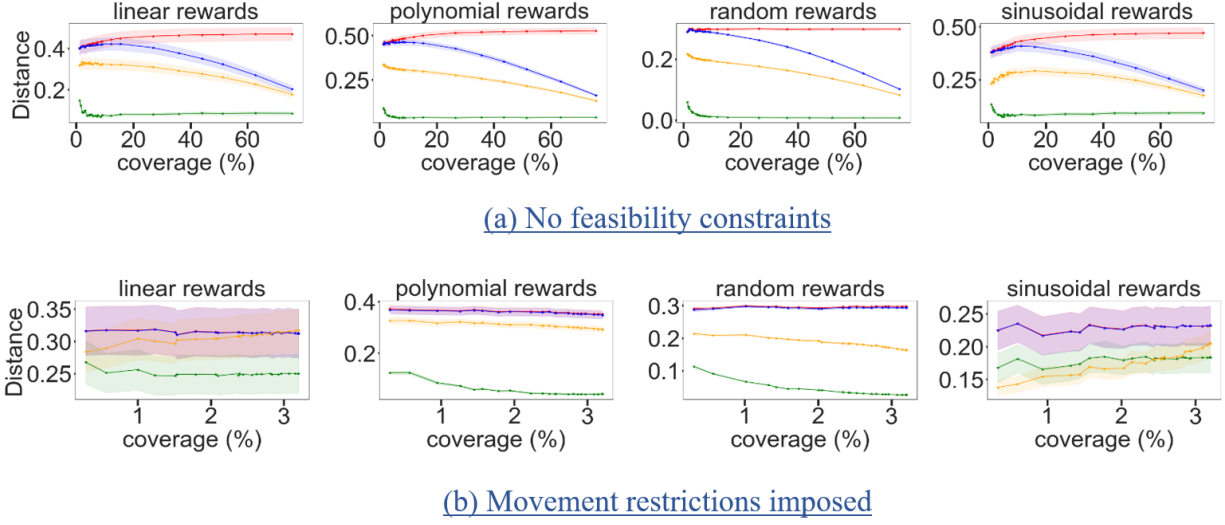
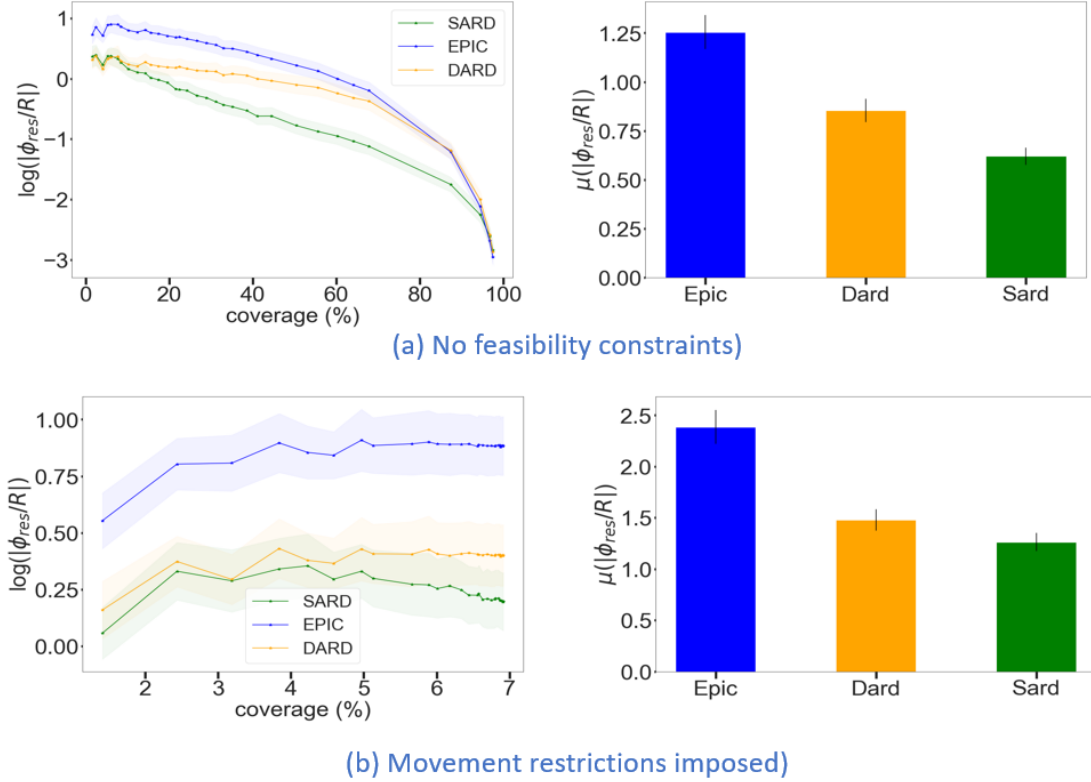
Parameter	Values
Rollout Counts, T	[1, 2, 3, 4, 5, 6, 7, 8, 9, 10, 15, 20, 30, 40, 50, 75, 100, 200, 300, 400, 500, 1000, 2000]
Epochs, E	200
Policy, π	uniform, $\epsilon = 0$
Discount, γ	0.7
Dimensions	20×20

B.4 Transition Sparsity: Additional Results

Parameter Variation In both the Gridworld and the Bouncing Balls domains, we did not see much difference in the structure of results between the 10×10 domain and the 20×20 domains. Results were fairly consistent in that SARD tends to outperform DARD and EPIC, and feasibility constraints tend to limit coverage significantly.

Figure 4: 10×10 Gridworld: Variation of reward relationships

Figure 5: 20 \times 20 Gridworld: Variation of reward relationshipsFigure 6: 10 \times 10 Bouncing Balls: Variation of reward relationships

Figure 7: 20×20 Bouncing Balls: Variation of reward relationshipsFigure 8: Here we compare the ratio of the residual potentials to the actual rewards for reward samples under comparison, on a 20×20 Bouncing Balls domain. As shown, SARD is less prone to residual shaping compared to DARD and EPIC.

B.5 Deviations from Potential Shaping

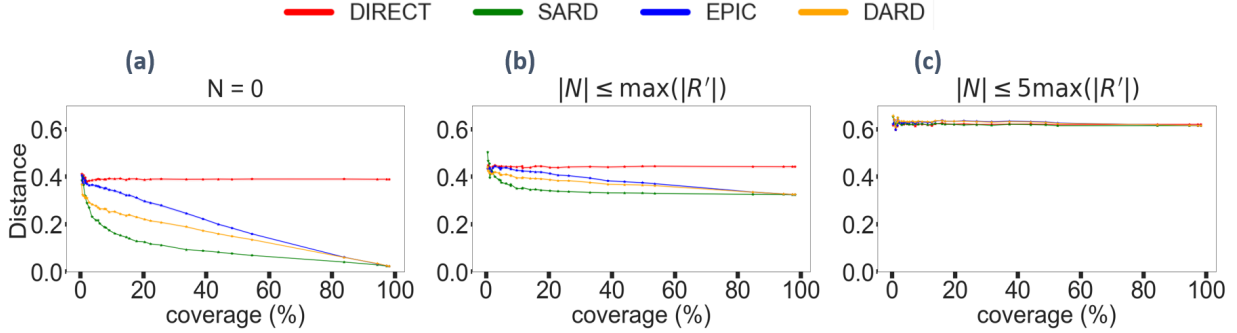


Figure 9: Non-Potential Shaping Effect: As the severity of randomly generated noise increases, rewards deviate more from potential shaping, hence all the pseudometrics degrade in performance. In the end, the pseudometrics perform to the level of DIRECT, showing that canonicalization does not yield any additional advantages at these levels.

Most reward comparison pseudometrics are designed with the goal of canonicalizing rewards that differ due to potential shaping. In this experiment, we examine how deviations from non-potential shaping can affect the performance of these pseudometrics. Within a 20×20 Gridworld domain, we generate a ground truth (GT) polynomial reward function and a corresponding shaped reward function (SH), both with full coverage (100% transitions). From GT and SH , we sample rewards R and R' using uniform policy rollovers. For both samples, we add additional noise, N , with the following severity levels: **None**: $N = 0$, **Mild**: $|N| \leq \max(|R'|)$, and **High**: $|N| \leq 5\max(|R'|)$, where N is randomly generated from a uniform distribution within bounds defined by these severity levels. Thus, the updated shaped reward is given by:

$$R'' = R' + N.$$

Figure 9 shows the performance variation of the reward comparison pseudometrics to the severity levels, dictated by N . As shown, when $N = 0$ (noise free), the difference between SARD, EPIC, DARD, and DIRECT is the greatest, with a performance order: $SARD > DARD > EPIC > DIRECT$, which demonstrates SARD’s performance advantage over other pseudometrics under potential shaping. As the impact of N increases, the shaped reward, R'' , becomes almost entirely comprised of noise, and the shaping component significantly deviates from potential shaping. As shown, SARD’s performance gap over other pseudometrics significantly diminishes. At high severity (Figure 9c), SARD’s performance is nearly identical to all other pseudometrics, including DIRECT, which does not involve any canonicalization. In conclusion, these results still demonstrate SARD’s superiority in canonicalizing rewards even with minor deviations from potential shaping (Figure 9 b). However, as the rewards become non-potentially shaped, all pseudometrics generally become ineffective, performing similarly to non-canonicalized techniques such as DIRECT.

C Experiment 2: Additional Analysis

C.1 Reward Classification: Testbeds and IRL

Gridworld: The Gridworld domain simulates agent movement from a given initial state to a specified terminal state under a static policy. Each state is defined by an (x, y) coordinate where $0 \leq x < N$, and $0 \leq y < M$ implying $|\mathcal{S}| = NM$. For Experiment 2, the action space only consists of four cardinal directions {north, east, south, west}, and to define classes, we use static policies based on the action-selection distribution (out of 100) per state. Table 1 shows the Gridworld parameters used for Experiment 2.

Bouncing Balls: The Bouncing Balls domain, adapted from (Wulfe et al., 2022), simulates a ball’s motion from a starting state to a target state while avoiding randomly mobile obstacles. These obstacles

add complexity to the environment since the ball might need to change its strategy to avoid obstacles (at a distance, $d = 3$). Each state is defined by the tuple (x, y, d) , where (x, y) indicates the ball’s current location, and d indicates the ball’s Euclidean distance to the nearest obstacle, such that: $0 \leq x < N$, $0 \leq y < M$, and $d \leq \max(M, N)$. The action space includes eight directions (cardinals and ordinals), with the stochastic parameter ϵ for choosing random transitions. Table 2 describes the parameters for Experiment 2.

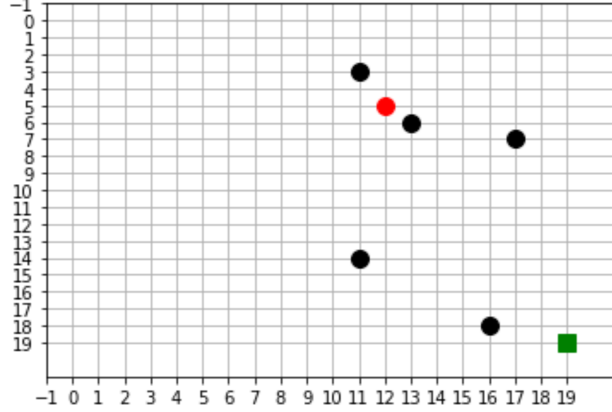


Figure 10: Bouncing Balls domain: The red ball starts at a randomly assigned state and aims to reach the green state while avoiding being close to the black obstacles. The presence of the obstacles makes the domain more complex than the simple Gridworld.

Drone Combat: The Drone Combat domain is derived from the multi-agent environment, which simulates a predator-prey interaction (Anurag, 2019). We adapt this testbed to simulate a battle between two drone swarms; a blue swarm denoting the ally team; and a red swarm denoting a default AI enemy. The goal is for the blue ally team to defeat the default AI team. This testbed offers discrete actions and states within a fully observable environment, while also offering flexibility for unit creation, and obstacle placement. However, the number of states and actions is still high such that we didn’t use it in Experiment 1. Each unit (blue and red squares) possesses a distinct set of parameters and possible actions. Each team consists of drones and ships, and the team that wins either destroys the entire drones of the opponent or its ship. This ship adds complexity to the decision-making process of the teams which need to engage with the enemy, as well as safeguard their ships. Each drone is defined by the following attributes: visibility range (VR) - the range a unit can see from its current position (partial observability); health (H) - the number of firings a unit can sustain; movement range(MR) - the maximum distance that a unit can move to; and shot strength(SS) - the probability of a shot hitting its target. All these attributes are drawn from the set:

$$U = \{(VR, H, MR, SS) \mid VR \in \{1, 3, 5\}, H \in \{5, 10, 15\}, MR \in \{1, 2, 3\}, SS \in \{0.05, 0.1\}\}$$

Table 5 summarizes the parameters used for Experiment 2.

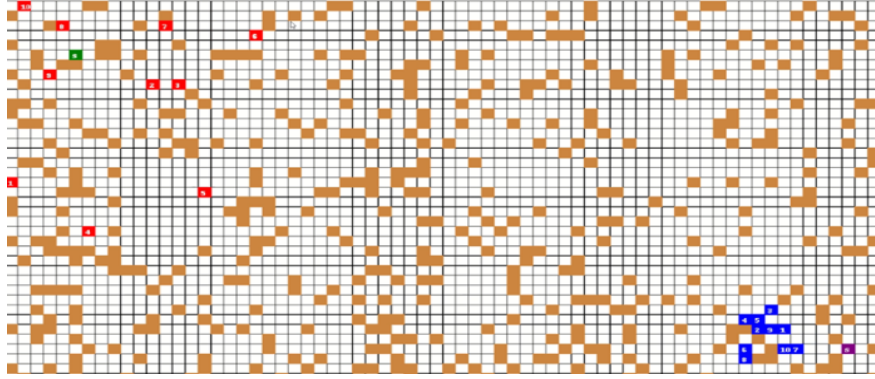


Figure 11: Drone Combat: The drone combat domain describes a battlefield scene where the blue team aims to attack the red AI team. The brown squares present movement obstacles; the green square represents the enemy’s ship; and the purple square represents the team’s ship.

Starcraft 2 (SC2): The SC2 domain is a strategy game created by Blizzard Entertainment that features real-time actions on a complex battlefield environment. The game involves planning, strategy, and quick decision-making to control a multi-agent ally team, aiming to defeat a default AI team in a competitive, challenging, and time-sensitive environment. SC2 serves not only as entertainment but also as a platform for professional player competitions. Due to its complexity and the availability of commonly used interactive Python libraries, the SC2 game is widely employed in Reinforcement Learning, serving as a testbed for multi-agent research. The goal of the ally team is to gather resources, and build attacking units that are used to execute a strategic mission to defeat the AI enemy; within an uncharted map, that gets revealed after extensive exploration (introduces partial observability). The sheer size of the map and the multitude of possible actions for each type of unit, as well as the number of units, contribute to the enormity of the action and state spaces. During combat, each ally unit, moves in a decentralized manner and attacks an enemy unit using an assigned cooperative strategy from the set: $C = \{c_1, c_2, c_3, c_4\}$; where c_1 - move towards ally closest to enemy’s start base; c_2 - move towards a random enemy unit; c_3 - move towards ally closest to an enemy unit; and c_4 - move towards the map’s center. We focus on attack-oriented ally units to reduce the state space. Non-attacking units such as pylons are treated as part of the environment. The game state records the number of ally units (num_{ally}), and the total number of opponent units (num_{enemy}); as well as the central coordinates of the ally and the enemy. The action records the number of ally units attacking the enemy at an instance. Table 6 describes the Starcraft 2 parameters used for Experiment 2.



Figure 12: (Starcraft 2): The domain describes a multiagent team that aims to defeat a default AI enemy. In this figure, the the red section denotes the team’s base where it builds resources and attacking units. In the green section, it shows the enemy’s base, where the team is attacking the enemy.

C.2 Testbed Parameters:

In all these domains, the optimal values for γ (discount factor) and k (the neighborhood size) are not fixed for each independent trial. Therefore, for hyperparameter selection, we employ a grid search over the set defined by:

$$\{(\gamma, k) : \gamma \in \{0, 0.1, \dots, 1\}, k \in \{5, 10, 15, \dots, 100\}\}$$

Table 4: Bouncing Balls parameters for Experiment 2.

Parameter	Values
Agent classes (10 classes)	[[12, 12, 12, 12, 13, 13, 13, 13], [5, 5, 25, 25, 25, 5, 5, 5], [25, 25, 25, 5, 5, 5, 5, 5], [5, 5, 5, 5, 5, 25, 25, 25], [5, 5, 65, 5, 5, 5, 5, 5], [5, 5, 5, 65, 5, 5, 5, 5], [5, 5, 5, 5, 65, 5, 5, 5], [5, 25, 5, 25, 5, 25, 5, 5], [20, 5, 20, 5, 20, 5, 20, 5], [5, 20, 5, 20, 5, 20, 5, 20]]
Trajectories generated per policy	100
Number of obstacles	5
Distance to deviate from obstacle (Manhattan)	3
Number of comparison trials	200
Actions	move: {north, north-east, east, east-south, south, south-west, west, west-north}
Dimensions	20×20

Table 5: Gridworld parameters for Experiment 2.

Parameter	Values
Agent classes (10 classes),	[[25, 25, 25, 25], [5, 5, 5, 85], [85, 5, 5, 5], [5, 85, 5, 5], [5, 5, 85, 5], [5, 15, 30, 55], [55, 30, 15, 5], [15, 5, 55, 30], [5, 55, 30, 15], [15, 30, 5, 55]]
Trajectories generated per policy,	100
Number of comparison trials,	200
Actions,	move: {north, west, south, east}
Dimensions	20×20 (400 states)

Table 6: Drone Combat parameters for Experiment 2.

Parameter	Values
Agent classes	10 classes, each consisting of 5 agents. Each agent x has attributes randomly drawn from the set: $U = \{(VR, H, MR, SS) \mid VR \in \{1, 3, 5\}, H \in \{5, 10, 15\}, MR \in \{1, 2, 3\}, SS \in \{0.05, 0.1\}\}$
Trajectories generated per policy	100
Number of agents per team	11 (1 ship, 10 drones)
Number of comparison trials	200
Actions, α denotes movement range, $1 \leq \alpha \leq 3$	$\{\text{left}^\alpha, \text{up}^\alpha, \text{right}^\alpha, \text{down}^\alpha\}, \text{attack}\}$
Dimensions	40×25 , with obstacles occupying $\approx 30\%$ of the area

Table 7: Starcraft 2 parameters for Experiment 2.

Parameter	Values
Agent classes (description in Starcraft 2 domain), generated based on resources and strategy	Class ratio of size 10, agents attributes: $U = \{(c, u) \mid c \in \{c_1, c_2, c_3, c_4\}, u \in \{\text{adept, voidray, phoenix, stalker}\}\}$.
Trajectories per policy	100
Comparison trials	200
Actions	Number of attacking units per unit time
State representation	$(num_{ally}, num_{enemy}, (x_{ally}, y_{ally}), (x_{enemy}, y_{enemy}))$

C.3 Inverse Reinforcement Learning (IRL)

In our experiments, we utilize Inverse Reinforcement Learning (IRL) to compute agent rewards based on demonstrated behavior. Specifically, we employ three IRL algorithms: Maximum Entropy IRL (Maxent-IRL) (Ziebart et al., 2008); Adversarial IRL; and Preferential Trajectory IRL (PT-IRL) (Santos et al., 2021). In addition, we compute manual rewards that differ due to potential shaping.

A trajectory $\tau_j = \{(s_0, a_0), (s_1, a_1), \dots, (s_d)\}$ is a sequence of states and actions. A set of trajectories can be written as:

$$\varphi = \{\tau_1, \tau_2, \dots, \tau_h\}, h \in \mathbb{Z}^+.$$

Maxent IRL The objective of the Maxent IRL⁶ algorithm is to compute a reward function that will generate a policy (learner) π_L that matches the feature expectations of the trajectories generated by the expert’s policy (demonstrations, assumed to be optimal) π_E . Formally, this objective can be expressed as:

$$\mathbb{E}_{\pi_L}[\phi(\tau)] = \mathbb{E}_{\pi_E}[\phi(\tau)], \quad (35)$$

where $\mathbb{E}_{\pi_k} = \sum_{\tau \in \varphi_k} p_{\pi_k}(\tau) \cdot \phi(\tau)$, and $p_{\pi_k}(\tau)$ is the probability distribution of selecting trajectory τ from π_k generated by the set of trajectories φ_k . Maxent IRL assumes that the relationship between state features and agent rewards is linear. To resolve the ambiguity of having multiple optimal policies which can explain an agent’s behavior, this algorithm applies the principle of maximum entropy to select rewards yielding a policy with the largest entropy.

AIRL: The AIRL algorithm uses generative adversarial networks to train a policy that can mimic the expert’s behavior. The IRL problem can be seen as training a generative model over trajectories as:

$$\max_w J(w) = \max_w \mathbb{E}_{\tau \sim \mathcal{D}}[\log p_w(\tau)], \quad (36)$$

where $p_w(\tau) \propto p(s_0) \prod_{t=0}^{T-1} P(s_{t+1}|s_t, a_t) e^{\gamma \cdot R_w(s_t, a_t)}$ and the parameterized reward is $R_w(s, a)$. Using the gradient of $J(w)$, the **entropy-regularized policy objective** can be shown to reduce to:

$$\max_{\pi} \mathbb{E}_{\pi} \left[\sum_{t=0}^T (R_w(s_t, a_t) - \log \pi(a_t|s_t)) \right] \quad (37)$$

The discriminator is designed to take the form:

$$D_w(s, a) = \frac{\exp\{f_w(s, a)\}}{\exp\{f_w(s, a)\} + \pi(a|s)}, \quad (38)$$

⁶Maxent and AIRL implementations adapted from: <https://github.com/HumanCompatibleAI/imitation> (Gleave et al., 2022)

and the **training objective** aims to minimize the cross-entropy loss between expert demonstrations and generated samples:

$$L(w) = \sum_{t=0}^T (-\mathbb{E}_{\mathcal{D}}[\log D_w(s_t, a_t)] - \mathbb{E}_{\pi_t}[\log(1 - D_w(s_t, a_t))]) \quad (39)$$

The policy optimization objective then uses the reward:

$$R(s, a) = \log(D_w(s, a)) - \log(1 - D_w(s, a)) \quad (40)$$

The AIRL formulation can be seen as an extension of the Guided Cost Learning (GCL) by Finn et al. (2016), with scalability modifications of analyzing data from a state-action level, rather than a trajectory-centric formulation. For example, in Finn et al. (2016), Equation 3.10 uses parameters $D_w(\tau)$ instead of $D_w(s, a)$. The AIRL formulation can also be shown to be equivalent to the Maxent IRL formulation.

PTIRL: The PTIRL algorithm incorporates multiple agents, each with a set of demonstrated trajectories φ_i . In order to compute the rewards for each agent, PTIRL considers target and non-target trajectories. Target trajectories are demonstrated trajectories from a target agent, and non-target trajectories are demonstrated trajectories from other agents. Denoting P_w as the probability transition function for all the agents, the linear expected reward for each trajectory τ is defined as

$$LER(\tau) = \sum_{k=1}^m P_w(s_k', a_k, s_k) \cdot r(s_k', a_k, s_k).$$

For each trajectory set, there is a lower bound value $lb(\varphi)$ and an upper bound value $ub(\varphi)$, respectively defined as

$$lb(\varphi) = \min_{\tau \in \varphi} (LER(\tau))$$

and

$$ub(\varphi) = \max_{\tau \in \varphi} (LER(\tau)).$$

With $lb(\varphi)$ and $ub(\varphi)$ definitions, the spread δ is defined as

$$\delta(\varphi_a, \varphi_b) = lb(\varphi_a) - ub(\varphi_b).$$

Preferential ordering for any two trajectories φ_a and φ_b is denoted by a poset, \prec , such that if $\varphi_b \prec \varphi_a$, then $\delta(\varphi_a, \varphi_b) > 0$.

Given the above definitions, let φ_i be the set of target trajectories and φ_{ni} the set of non-target trajectories. Assuming that the rewards of the target agent will ensure its behavior towards the target trajectories, the PT-IRL objective is to find rewards such that $\varphi_{nt} \prec \varphi_i$, $\delta(\varphi_i, \varphi_{nt}) \geq \alpha$, where α is the minimum threshold for the spread. PT-IRL is generally fast because it directly computes rewards via linear optimization.

C.4 Reward Classification: Additional Results

Table 8: Experiment 2: Welch’s t-tests

Domain	Rewards	SARD_vs_DIRECT		SARD_vs_EPIC		SARD_vs_DARD	
		t-statistic	p-value	t-statistic	p-value	t-statistic	p-value
Gridworld	Manual	11.522	0	12.478	0	10.385	0
	Maxent	28.496	0	28.142	0	2.593	0.005
	AIRL	13.610	0	5.117	0	4.266	0
	PTIRL	11.209	0	5.719	0	7.725	0
Bouncing Balls	Manual	18.801	0	17.375	0	6.955	0
	Maxent	32.341	0	12.104	0	-2.586	0.995
	AIRL	45.020	0	28.226	0	19.488	0
	PTIRL	5.089	0	3.101	0.001	7.096	0
Drone Combat	Manual	16.152	0	15.851	0	16.786	0
	Maxent	17.829	0	-2.543	0.994	9.123	0
	AIRL	9.772	0	8.023	0	3.935	0
	PTIRL	61.534	0	34.679	0	30.384	0
Starcraft 2	Manual	24.419	0	20.633	0	15.760	0
	Maxent	6.171	0	1.717	0.043	2.233	0.013
	AIRL	4.992	0	4.300	0	-2.913	0.998
	PTIRL	6.054	0	3.631	0	4.961	0

In Table 8, we show the comprehensive results for the Welch’s t-tests for unequal variances, which are conducted across all domain and reward type combinations, to test the null hypotheses: (1) $\mu_{SARD} \leq \mu_{DIRECT}$, (2) $\mu_{SARD} \leq \mu_{EPIC}$, and (3) $\mu_{SARD} \leq \mu_{DARD}$; against the alternative: (1) $\mu_{SARD} > \mu_{DIRECT}$, (2) $\mu_{SARD} > \mu_{EPIC}$, and (3) $\mu_{SARD} > \mu_{DARD}$, where μ represents the sample mean. Generally, the tests indicate that (1) $\mu_{SARD} > \mu_{DIRECT}$ for all instances; (2) $\mu_{SARD} > \mu_{EPIC}$ for 11 out of 12 instances, and (3) $\mu_{SARD} > \mu_{DARD}$ for 10 out of 12 instances. These tests are performed at a significant level of $\alpha = 0.05$, assuming normality as per central limit theorem, since the number of trials is 200. In summary, we conclude that the SARD pseudometric is more effective at classifying reward samples compared to its baselines. Full details on accuracy scores collected are shown in Table 9 and Table 10.

Table 9: Experiment 2: Accuracy results

Domain	Rewards	Statistic	DIRECT	EPIC	DARD	SARD
Gridworld	Manual	mean	69.8	69.3	70.0	75.8
		stdev	4.6	4.6	5.0	4.6
	Maxent	mean	57.4	57.5	68.9	70.0
		stdev	4.5	4.5	4.5	4.4
	AIRL	mean	82.3	84.9	85.0	86.2
		stdev	3.0	1.8	2.6	2.7
	PTIRL	mean	82.2	84.2	83.4	86.0
		stdev	3.5	3.3	3.5	3.3
Bouncing Balls	Manual	mean	46.5	47.3	52.0	55.2
		stdev	4.8	4.6	4.8	4.5
	Maxent	mean	39.7	46.0	50.8	49.9
		stdev	3.1	3.3	3.2	3.2
	AIRL	mean	41.2	46.1	49.8	56.3
		stdev	3.4	3.9	3.3	3.3
	PTIRL	mean	70.3	71.1	69.5	72.4
		stdev	4.2	4.3	4.1	4.0
Drone Combat	Manual	mean	67.1	67.2	66.2	73.9
		stdev	4.1	4.2	4.9	4.2
	Maxent	mean	70.3	77.7	73.2	76.8
		stdev	3.7	3.8	4.2	3.5
	AIRL	mean	90.1	90.7	92.3	93.8
		stdev	3.9	3.9	3.7	3.7
	PTIRL	mean	52.5	63.7	65.1	78.3
		stdev	4.3	4.3	4.6	4.1
Starcraft 2	Manual	mean	65.5	67.4	69.5	76.5
		stdev	4.6	4.5	4.5	4.4
	Maxent	mean	72.3	74.1	73.9	74.8
		stdev	4.1	4.1	4.2	4.1
	AIRL	mean	75.1	75.3	78.1	77.0
		stdev	4.0	4.0	3.8	3.8
	PTIRL	mean	77.2	78.1	77.6	79.6
		stdev	4.1	4.2	4.2	4.0

Table 10: Experiment 2: Precision, Recall, F1-scores

Domain	Rewards	Statistic	DIRECT			EPIC			DARD			SARD		
			precision	recall	f1-score	precision	recall	f1-score	precision	recall	f1-score	precision	recall	f1-score
Gridworld	Maxent	mean	64.7	57.6	56.8	64.8	57.7	56.9	72.9	68.8	67.8	76.1	70.1	69.6
		stdev	3.5	4.1	4.1	3.4	4.0	4.0	3.7	4.9	4.8	3.6	4.3	4.2
	Manual	mean	74.4	70.0	68.8	73.6	69.4	68.1	74.0	70.1	68.4	78.7	76.1	73.2
		stdev	4.1	4.4	4.7	4.5	4.4	4.8	4.5	4.5	4.9	4.2	3.3	4.2
	AIRL	mean	77.5	82.5	78.3	85.9	85.2	84.0	78.3	85.5	81.0	81.1	86.4	82.5
		stdev	2.3	1.9	2.3	1.5	1.1	1.7	2.1	1.5	1.8	1.9	1.7	1.9
	PTIRL	mean	77.9	82.3	77.9	80.4	84.2	79.8	78.0	83.6	78.8	82.5	86.4	81.8
		stdev	5.5	2.8	3.0	5.1	2.2	2.7	4.8	2.4	2.9	5.7	2.2	2.8
	Bouncing Balls	mean	44.6	46.3	39.7	45.2	47.3	40.5	46.8	52.4	44.0	52.7	55.7	45.8
		stdev	7.1	3.9	4.4	7.0	3.6	4.1	6.4	3.3	4.0	7.0	2.7	3.9
Drone Combat	Manual	mean	33.5	39.7	34.1	41.1	45.9	40.9	51.1	50.6	47.3	42.9	49.8	42.4
		stdev	2.6	2.3	2.0	3.1	2.6	2.4	5.6	3.0	3.1	3.4	2.8	2.8
	AIRL	mean	35.0	41.2	35.7	45.0	46.1	43.1	49.6	50.1	46.6	58.4	56.7	50.9
		stdev	3.0	2.7	2.7	3.8	3.0	3.0	3.4	2.8	2.9	5.6	2.3	3.1
	PTIRL	mean	67.4	69.7	64.3	69.2	70.5	65.1	64.2	69.0	61.8	65.4	71.9	66.2
		stdev	6.4	2.7	3.8	6.4	2.7	3.8	6.4	2.7	3.8	5.1	2.8	3.5
	Maxent	mean	64.1	67.1	60.5	67.1	67.0	64.0	65.1	66.3	62.7	67.4	73.1	70.2
		stdev	4.0	4.1	4.0	3.9	4.1	4.0	5.0	3.9	4.4	4.5	4.2	4.3
	AIRL	mean	65.1	70.3	67.6	74.1	77.6	72.8	74.6	73.5	71.0	74.0	76.6	71.3
		stdev	3.8	3.6	3.7	3.6	3.8	3.7	4.5	3.2	3.8	4.0	3.5	3.7
Starcraft 2	Manual	mean	90.0	90.1	89.0	88.2	90.4	89.3	90.2	92.5	86.3	92.2	93.6	91.9
		stdev	4.0	3.9	3.9	3.8	4.0	3.9	4.2	3.8	4.0	3.6	3.6	3.6
	PTIRL	mean	50.2	52.5	48.3	60.4	64.3	60.7	63.1	65.0	64.6	79.3	77.7	78.5
		stdev	4.8	4.3	4.5	4.6	4.4	4.8	4.7	4.4	4.4	4.5	4.0	4.2
	Maxent	mean	60.2	65.4	62.7	64.1	67.3	64.7	70.1	69.2	67.9	76.1	76.9	74.5
		stdev	4.5	4.6	4.5	4.8	4.4	4.6	4.5	3.5	3.9	4.7	4.3	4.5
	AIRL	mean	73.1	72.2	69.6	70.4	74.1	70.2	69.1	73.2	70.1	72.7	74.7	73.7
		stdev	4.0	4.1	4.0	4.5	4.5	4.3	4.4	4.2	4.1	4.0	4.2	4.1
	PTIRL	mean	73.8	75.0	70.4	73.9	73.8	69.8	76.7	77.9	73.7	76.8	78.6	76.7
		stdev	3.7	4.0	3.8	4.3	3.9	4.1	3.9	3.9	3.9	3.9	4.0	3.9
Starcraft 2	PTIRL	mean	72.1	77.1	72.5	77.6	78.6	77.1	78.1	77.0	75.7	80.0	79.5	76.7
		stdev	3.9	4.1	4.0	4.2	4.3	4.4	4.5	4.3	4.2	4.0	3.9	4.0